Electronic Supplementary Material (ESI) for ChemComm.
This journal is © The Royal Society of Chemistry 2022

Supporting information

Polymer networks of imine-crosslinked metal-organic cages: tuneable viscoelasticity and iodine adsorption

Matthew L. Schneider,[a] Jonathan A. Campbell[b], Ashley D. Slattery[c] and Witold M. Bloch*[a,b]

[a]Department of Chemistry, The University of Adelaide, Adelaide, Australia.

[b]Institute for Nanoscale Science and Technology, College of Science and Engineering, Flinders University, Bedford Park, South Australia 5035, Australia.

[c]Adelaide Microscopy, The University of Adelaide, Adelaide 5005, Australia

Email: wit.bloch@flinders.edu.au

Contents

1 Experimental

1.1 General Methods

Unless otherwise stated, all chemicals were obtained from commercial sources and used as received. Anhydrous DMSO (Merck) was dispensed under N_2 for all relevant experiments. Tetrahydrofuran (THF) was freshly distilled using a sodium/benzophenone solvent still. Diformyl benzene (**dfb**) and 4,4'-biphenyldicarboxaldehyde (**bpc**) standard solutions (165 mM) were prepared in dry DMSO. A standard solution of $Sc(OTf)_3$ (40 mg, 1 mL dry DMSO, 81 mM) was used for all cross-linking experiments. UV-Vis absorbance data was collected on a PS Shimdazu UV-3600Plus using 1 mL cells.

Powder X-ray diffraction data were collected on a Bruker Advanced D8 diffractometer (capillary stage) using Cu Kα radiation (λ = 1.5418 Å, 50 kW/40mA) Simulated powder X-ray diffraction patterns were generated from the single crystal data using Mercury 4.3.1 TEM imaging of MOP-15 was performed on an FEI Tecnai G2 Spirit TEM operated at 120 kV. A solution of MOP-15 was combined with EtOH before being dispersed onto a carbon TEM grid. TEM imaging of **G102** was performed using a probe-corrected, low-base FEI Titan Themis 80-200 (FEI, Hillsboro, OR, USA) operated at 200 kV with an X-FEG Schottky source. A dried sample of **G102** was dispersed into EtOH before being loaded onto a carbon TEM grid. Strain sweep experiments were run from 0.5% to 50% at 25 °C to determine an adequate strain %, recorded on the TA Instruments AR 2000. Frequency sweep experiments were performed from 0.1 rad/s to 100.0 rad/s at a strain rate of 5% (at 25 °C); the storage and loss modulus were recorded by a TA Instruments AR 2000. All experiments utilised the TA Instruments 25 mm ETC aluminium parallel plate.

EGTA digestion solution – Egtazic acid (EGTA) (100 mg, 0.262 mmol) was added to dry DMSO-d_6 (800 μL) followed by the addition of Tetrabutylammonium hydroxide (1 mL, 1M in MeOH). The solution was heated at 65 °C for 25 minutes until all reagents had dissolved. The solution was stored at 25 °C.

Digestion protocol of G10X / G20X – A portion of the G10X / G20X gel (extracted via micro spatula) was removed from the reaction vessel and submerged in 650 μL of DMSO-d_6. The EGTA digestion solution (50 μL) was added and the reaction vial was gently shaken until all the material had dissolved. ^{1}H NMR spectra were recorded typically within 5-10 minutes of dissolution (refer to figure S12 for stability control experiment).

1.2 Synthesis

1.2.1 Synthesis of MOP-15

In a screw-cap vial, 5-NH_2-bdc (10 mg, 0.055 mmol) was combined with $Cu(OAc)_2 \cdot H_2O$ (12 mg, 0.061 mmol) in 1 mL of dry DMSO at 25 °C. After 5 minutes, a DMSO solution of MOP-15 was obtained. Green rectangular crystals of MOP-15 could be obtained by leaving the vial to stand for 7 days.

1.2.2 Synthesis of Cu_{24}(5-MeCONH-bdc)$_{24}$

In a screw-cap vial 5-NH_2-bdc (10 mg, 0.055 mmol) was combined with $Cu(OAc)_2 \cdot H_2O$ (12 mg, 0.061 mmol) in 1 mL of dry DMSO at 25 °C. After 5 minutes, acetic anhydride (16.8 mg, 0.165 mmol) was added in one portion and the reaction mixture was left to stand for 12 hours. Slow vapor diffusion of MeOH into the DMSO solution afforded blue rectangular crystals of Cu_{24}(5-MeCONH-bdc)$_2$.

1.2.3 General procedure for preparation of G10X

To a solution of 5-NH_2-bdc (10 mg, 0.055 mmol) in dry DMSO (800 μL), $Cu(OAc)_2 \cdot H_2O$ (12 mg, 0.061 mmol) was added and the mixture was sonicated until complete dissolution and left to stand for 15 minutes. An aliquot of diformyl benzene (**dfb**) solution (refer to Table S1) was added. The appropriate amount of dry DMSO was added to reach a volume of 1 mL. $Sc(OTf)_3$ in DMSO (25 μL, 0.000121 mmol, 81 mM) was added and the vial was left to stand at 25 °C for 6 hours.

1.2.4 General procedure for preparation of G20X

To a solution of 5-NH_2-bdc (10 mg, 0.055 mmol) in dry DMSO (800 μL), $Cu(OAc)_2 \cdot H_2O$ (12 mg, 0.061 mmol) was added and the mixture was sonicated until complete dissolution and left to stand for 15 minutes. An aliquot of 4,4'-biphenyldicarbaldehyde (**bpc**) solution (refer to Table S1) was added in one portion. The appropriate amount of dry DMSO was added to reach a volume of 1 mL. $Sc(OTf)_3$ in DMSO (25 μL, 0.000121 mmol, 81 mM) was added and the vial was left to stand at 25 °C for 6 hours.

1.2.5 G10X and G20X table of reagents.

Table S1: Equivalents of aldehyde linker required for G10X and G20X gels.

Aldehyde linker (std. solutions in DMSO, 165 mM)	Equivalent (molar eq to 5-NH_2-bdc	Volume of std. solution (μL)
dfb	**0.1 / 0.2 / 0.3** / 0.5 / 0.6	**33 / 66 / 100** / 165 / 200
bpc	**0.1 / 0.2 / 0.3**	**33 / 66 / 100**

* The bolded values indicate **G101** (0.1 equiv.), **G102** (0.2 equiv.) and **G103** (0.3 equiv.) respectively (same trend for the G20X series). The larger equivalents were synthesised for control experiments (*vide infra*).

1.2.6 Control experiments for MOP-15 polymer network formation

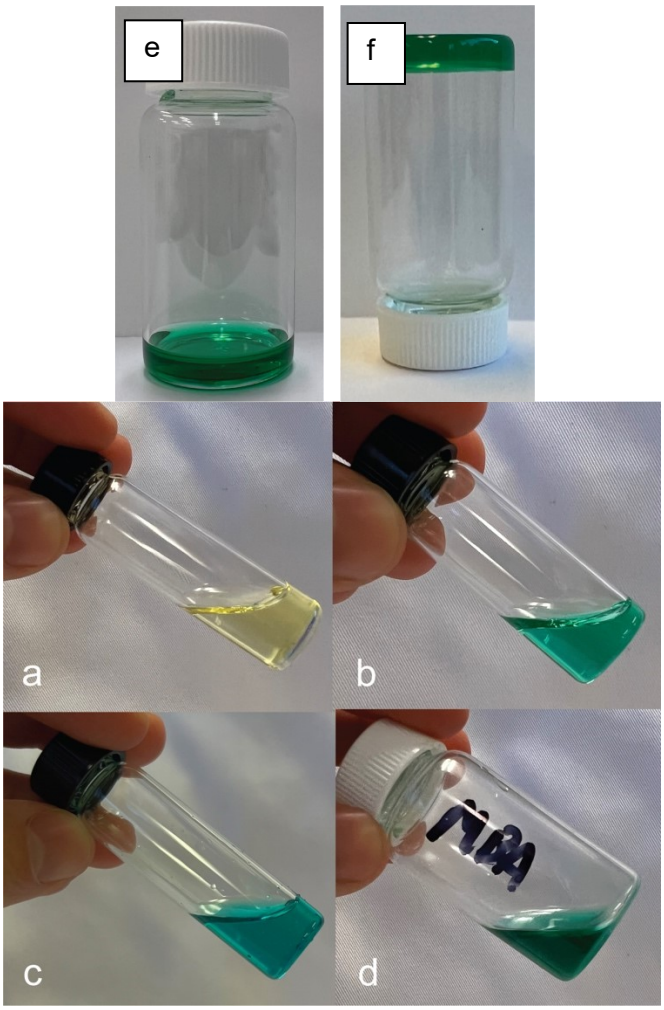

Figure S1. Control experiments showing that gelation/crosslinking does not occur if one of the components is omitted (eg., $Cu(OAc)_2$, $Sc(OTf)_3$ or 5-NH_2-bdc): a) no $Cu(OAc)_2$, b) no $Sc(OTf)_3$, c) no 5-NH_2-bdc and finally d) a mixture of m-carboxyaniline + $Cu(OAc)_2$ + $Sc(OTf)_3$ and dfb. The absence of gel formation in the latter sample indicates that the presence of MOP-15 is required to form the organogel product; e) $Cu(OAc)_2$, 5-NH_2-bdc and $Sc(OTf)_3$; f) $Cu(OAc)_2$, 5-NH_2-bdc and $Sc(OTf)_3$, followed by the addition of dfb after 15 min.

1.3 Characterisation

1.3.1 Formation of MOP-15; ^{1}H NMR spectroscopy

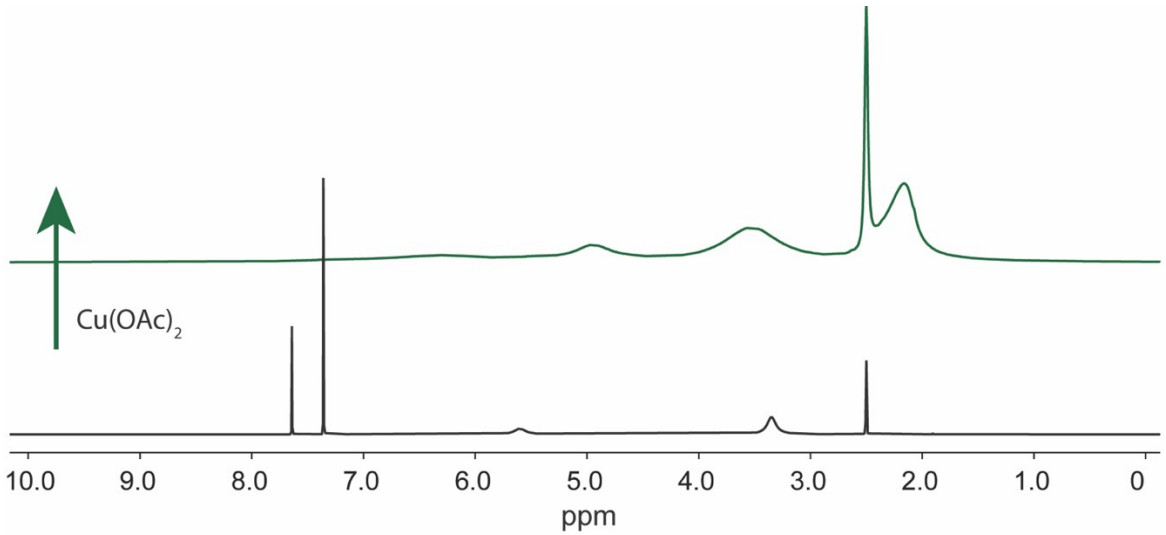

Figure S2. ^{1}H NMR (500 MHz, DMSO-d_6) spectrum of 5-NH_2-bdc before and after the addition of $Cu(OAc)_2$ (10 min). The disappearance of 5-NH_2-bdc signals and the broadness after the addition of Cu^{II} indicate coordination of 5-NH_2-bdc to Cu^{II}.

1.3.2 Formation of MOP-15; UV-Vis Spectroscopy

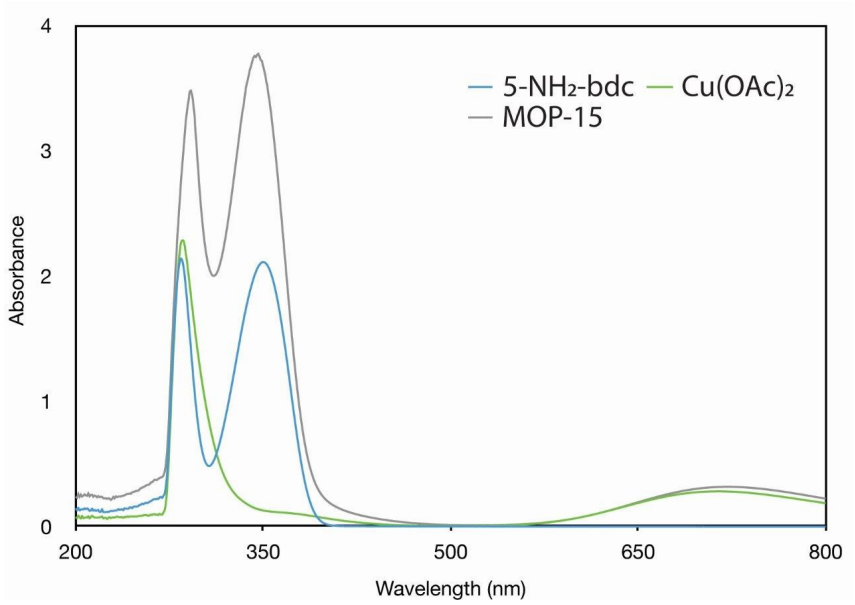

Figure S3. UV-Vis spectrum of 5-NH_2-bdc, $Cu(OAc)_2$ and MOP-15 (obtained directly after adding 5-NH_2-bdc to $Cu(OAc)_2$ in DMSO). Shifting of the maxima absorption peak in the copper paddlewheel region (600 – 800) is consistent with the formation of the Cu_{24}(5-NH_2-bdc)$_{24}$ metal-organic cage.

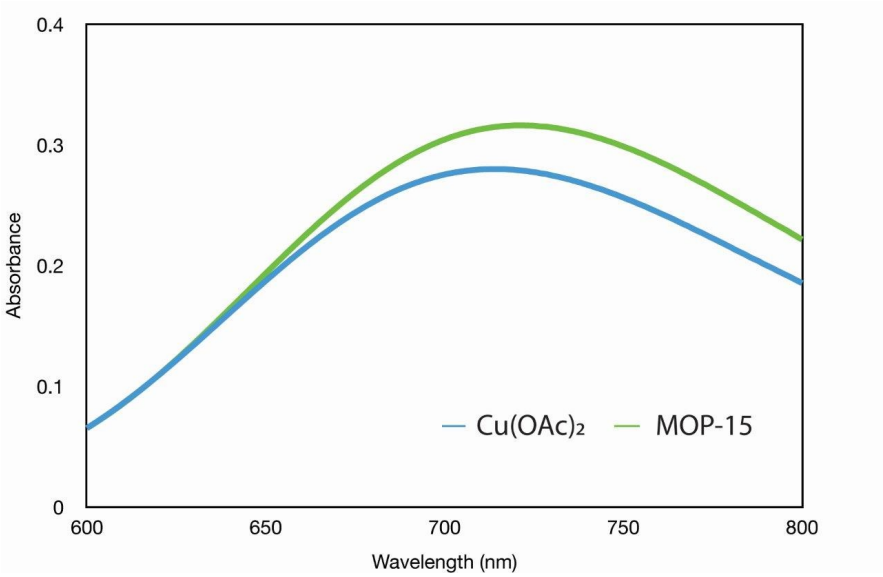

Figure S4. UV-Vis spectrum of $Cu(OAc)_2$ and MOP-15 (obtained directly after adding 5-NH_2-bdc to $Cu(OAc)_2$ in DMSO). Shifting of the maxima absorption peak in the copper paddlewheel region (600 – 800) is consistent with the formation of the Cu_{24}(5-NH_2-bdc)$_{24}$ metal-organic cage.

1.3.3 DLS data of MOP-15

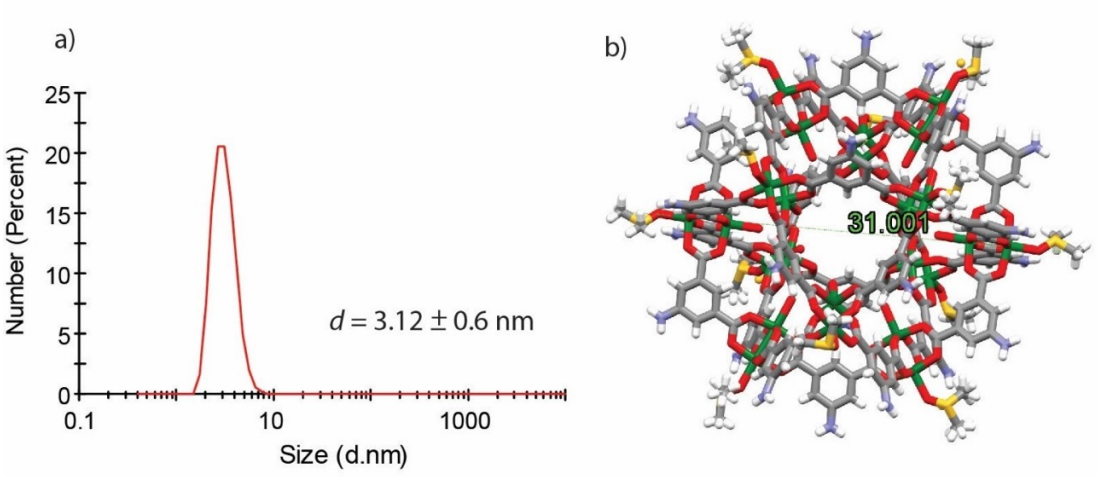

Figure S5. a) Dynamic light scattering of a DMSO solution of MOP-15 obtained 10 minutes after mixing $Cu(OAc)_2$ and 5-NH_2-bdc. b) X-ray structure of MOP-15-DMSO. The theoretical diameter of MOP-15 is shown (31 Å, m measured across the molecule from DMSO carbon to DMSO carbon)

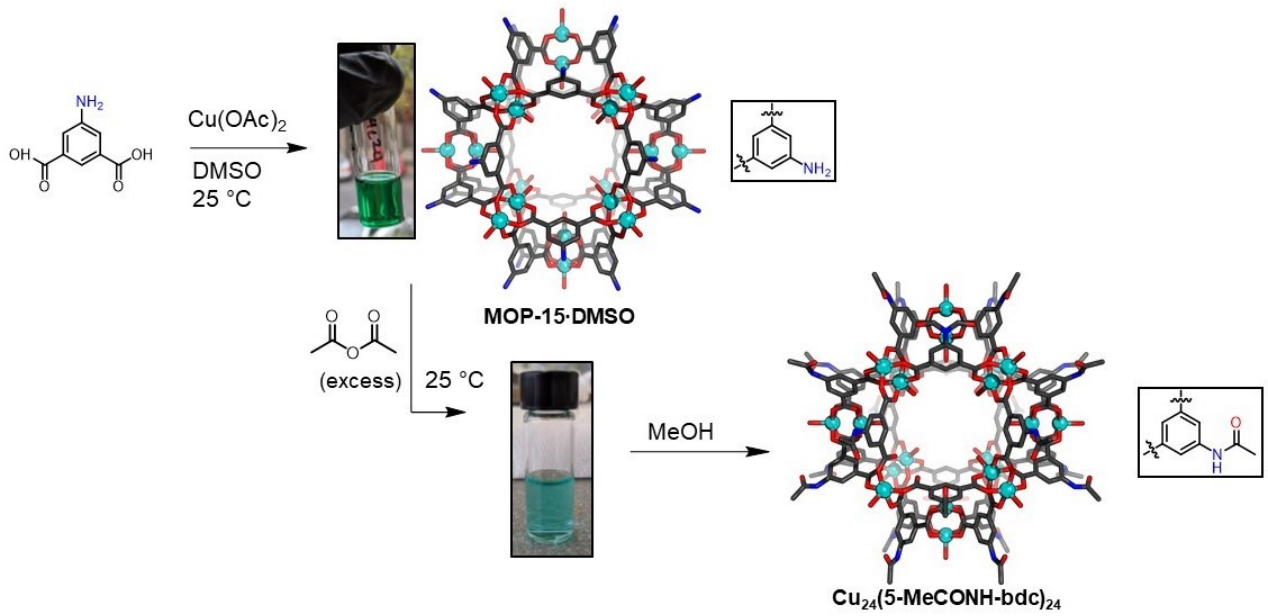

Figure S6. Reaction of MOP-15 with acetic anhydride, showing X-ray structures of MOP-15 (disordered DMSO removed for clarity) and Cu_{24}(5-MeCONH-bdc)$_{24}$. Slow-vapour diffusion of MeOH produces crystals of Cu_{24}(5-MeCONH-bdc)$_{24}$.

1.3.4 Digestion and assignment of protons in G10X and G20X

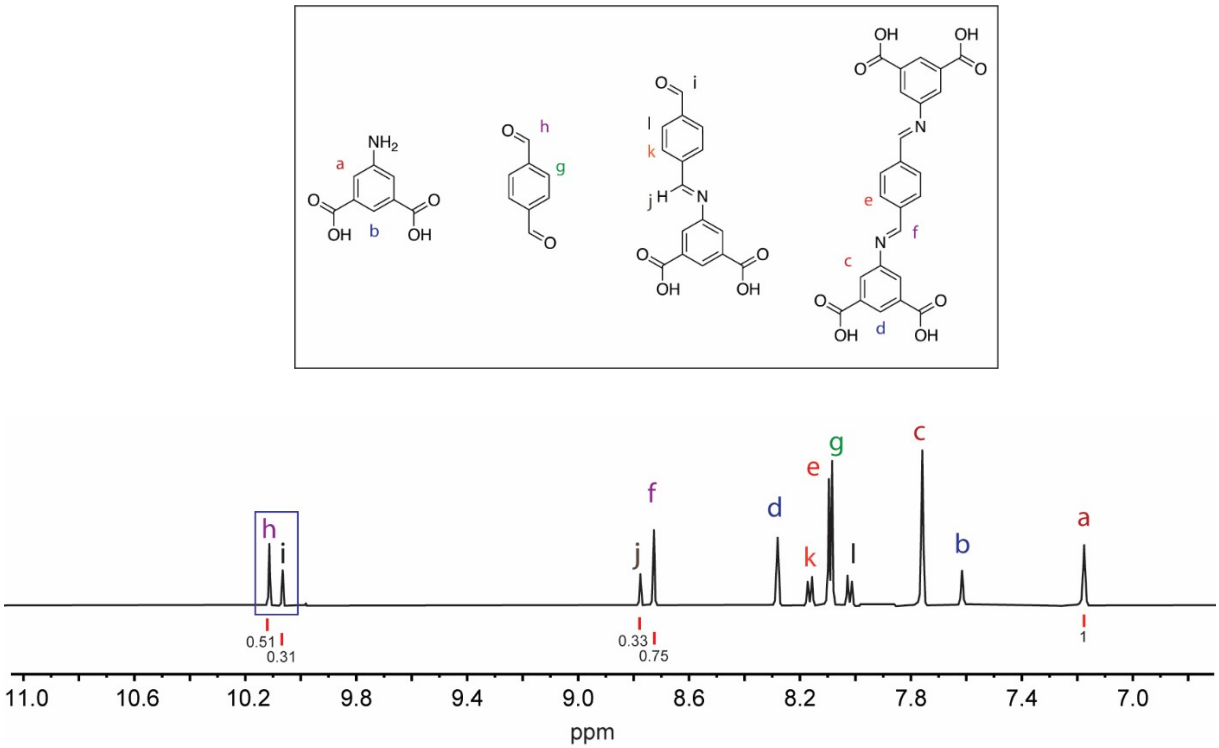

Figure S7. ^{1}H NMR (500 MHz, DMSO-d_6) spectrum of the digestion and assignment of **G105**. The ^{1}H NMR spectrum reveals larger integrations of the mono-condensed imine and aldehyde protons (i and j; see figure S9) compared to the remainder of the G10X series.

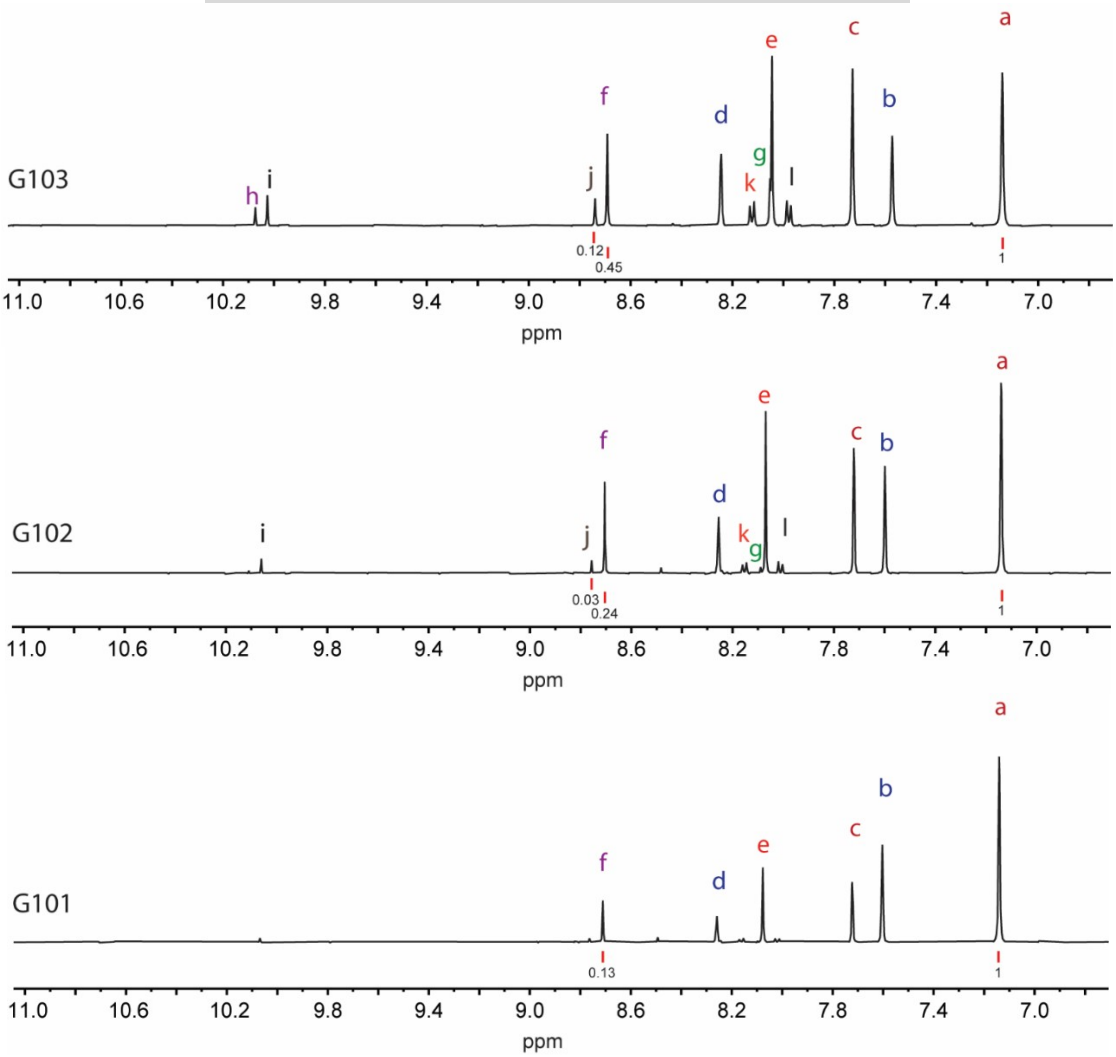

Figure S8. ^{1}H NMR (500 MHz, DMSO-d_6) spectra of G10X samples digested with EGTA solution.

Table S2: Integrations of the imine C-H protons from the digestion experiments of G10X (^{1}H NMR spectroscopy) along with the calculated branch functionality. The unreacted ligand (*a* in above spectra) is set to '1' for integration purposes.

	G101	**G102**	**G103**
Mono-imine	ND	0.03	0.12
Di-imine	0.13	0.24	0.45
Branch Functionality	2.6	4.6	6.5

$$crosslinking\ (\%) = \frac{a}{(a+b+c)} * 100. \qquad branch\ functionality = crosslinking\ (\%) * 24$$

Where a = di-imine integration, b = unreacted ligand integration and c = mono-imine integration of equal protons (if present in data). ND = none detected

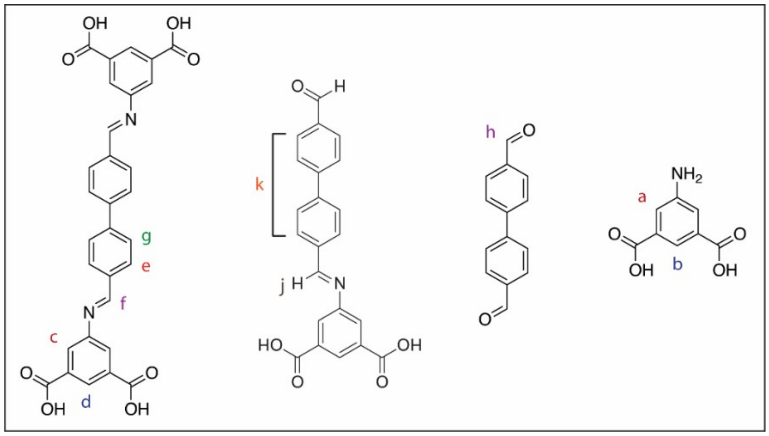

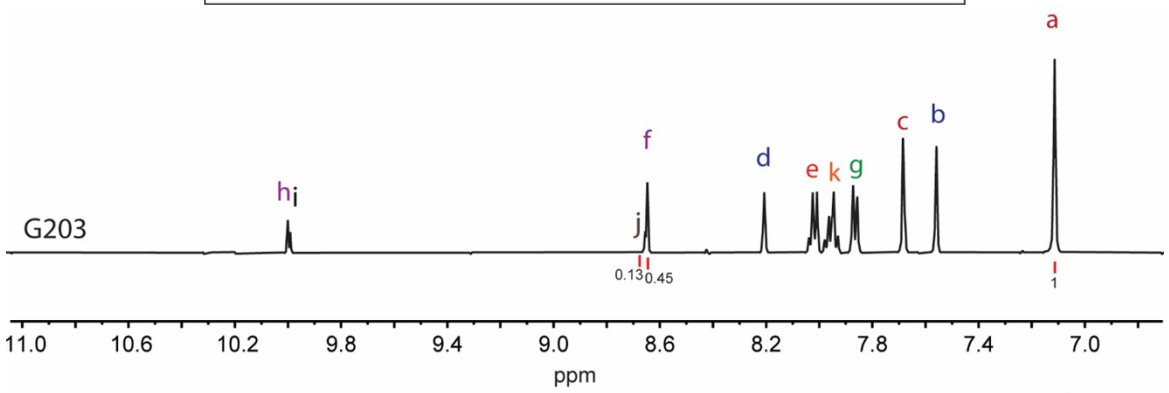

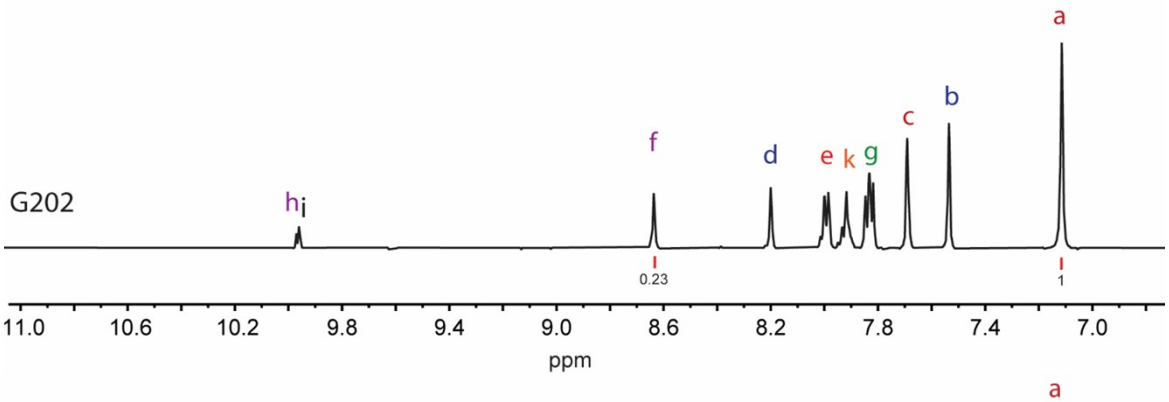

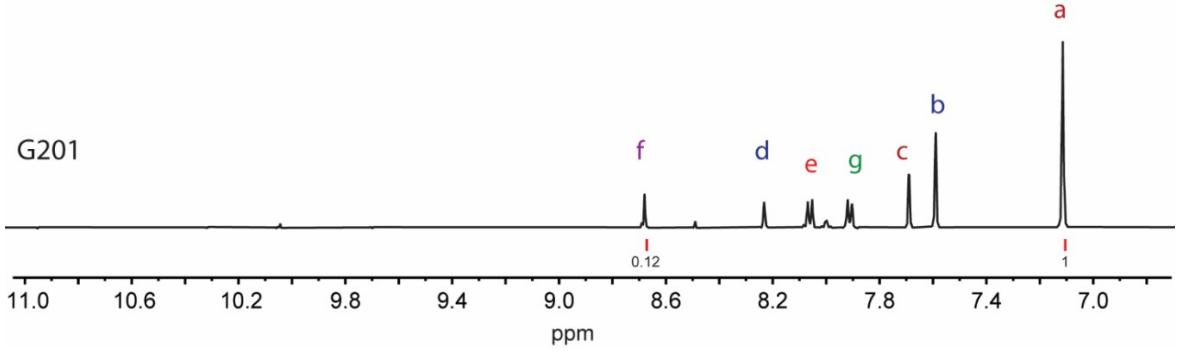

Figure S9. ^{1}H NMR (500 MHz, DMSO-d_6) spectra of G20X samples digested with EGTA.

Table S3: Integrations of the imine C-H protons from the digestion experiments of G20X (^{1}H NMR spectroscopy) along with the calculated branch functionality. The unreacted ligand (*a* in above spectra) is set to '1' for integration purposes.

	G201	G202	G203
Mono-imine	ND	ND	0.13
Di-imine	0.12	0.23	0.45
Branch Functionality	2.6	4.6	6.3

ND = none detected

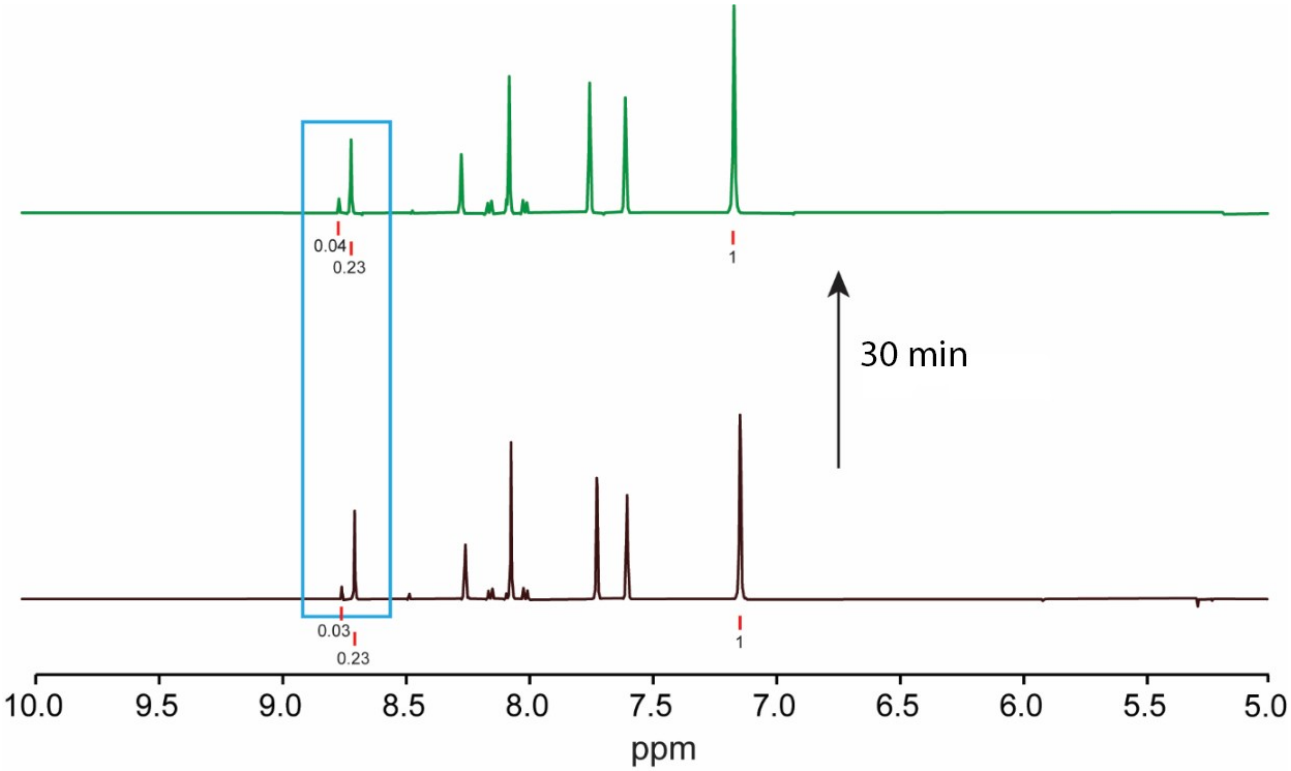

Figure S10. ^{1}H NMR (500 MHz, DMSO-d_6) spectrum of an EGTA digestion of G102 at time = 5 min (bottom) and time = 30 minutes (top). The integrations of the imine peaks highlighted in the blue rectangle do not significantly change over this time period. Thus, the EGTA digestion solution does not reverse the imine bonds over time.

2. Powder X-ray diffraction (PXRD)

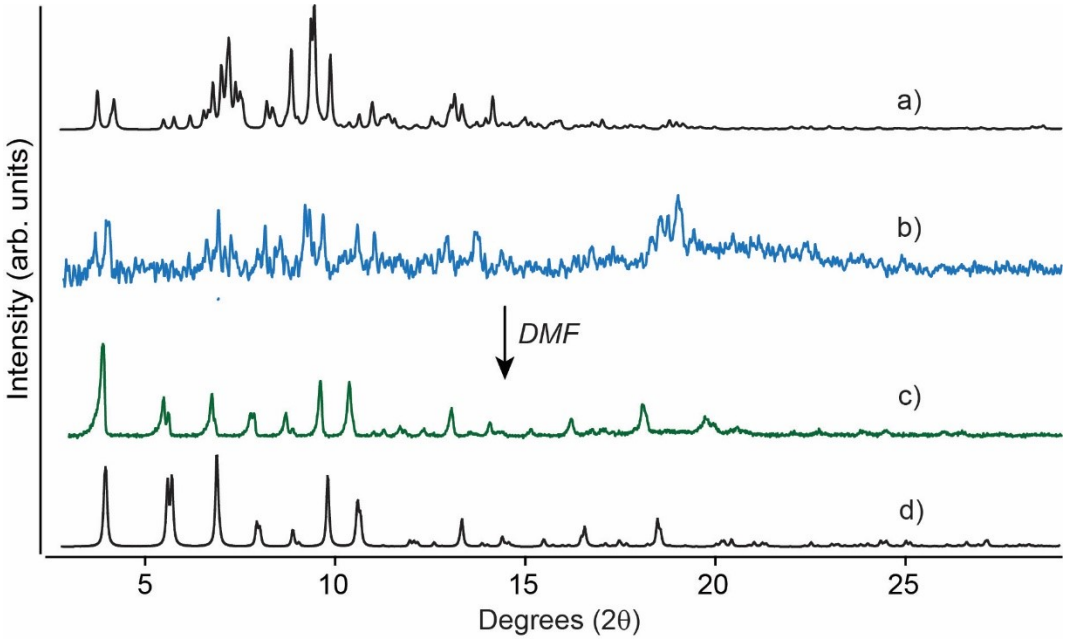

Figure S11. Powder x-ray diffraction (PXRD) patterns: a) MOP-15·DMSO (simulated); b) MOP-15·DMSO (experimental); c) MOP-15·DMSO crystals suspended in DMF after 30 mins; d) MOP-15 (simulated) as reported by Yaghi.[1] Note: despite repeated attempts (increased exposure time and trails with multiple samples), better quality PXRD patterns of MOP-15·DMSO could not be obtained.

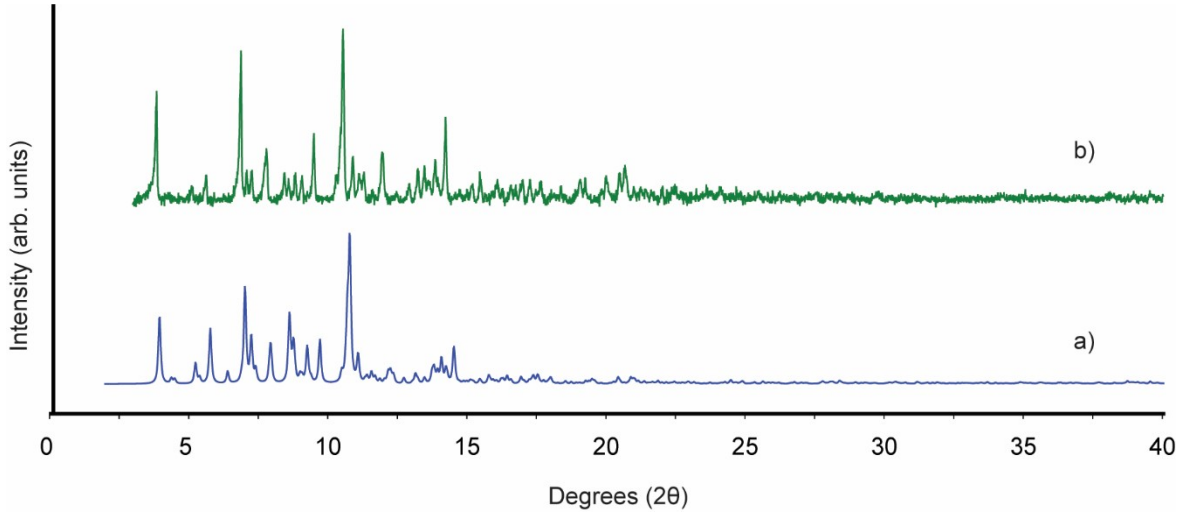

Figure S12. Powder x-ray diffraction (PXRD) patterns of a) Cu_{24}(5-MeCONH-bdc)$_{24}$ (simulated) and b) Cu_{24}(5-MeCONH-bdc)$_{24}$ (experimental).

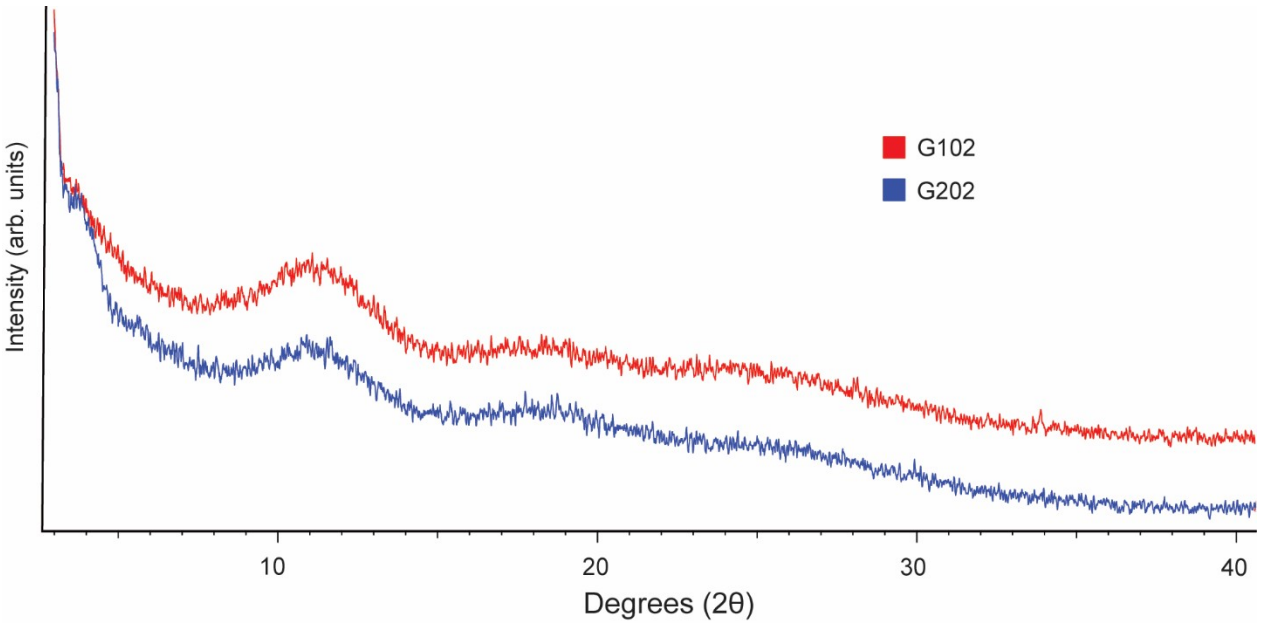

Figure S13. Powder X-ray diffraction (PXRD) patterns G102 and G202 as synthesized. All other MOC-polymer samples are equally amorphous.

3. Small Angle X-ray Scattering (SAXS)

3.1. G102 / G202 gel formation over time

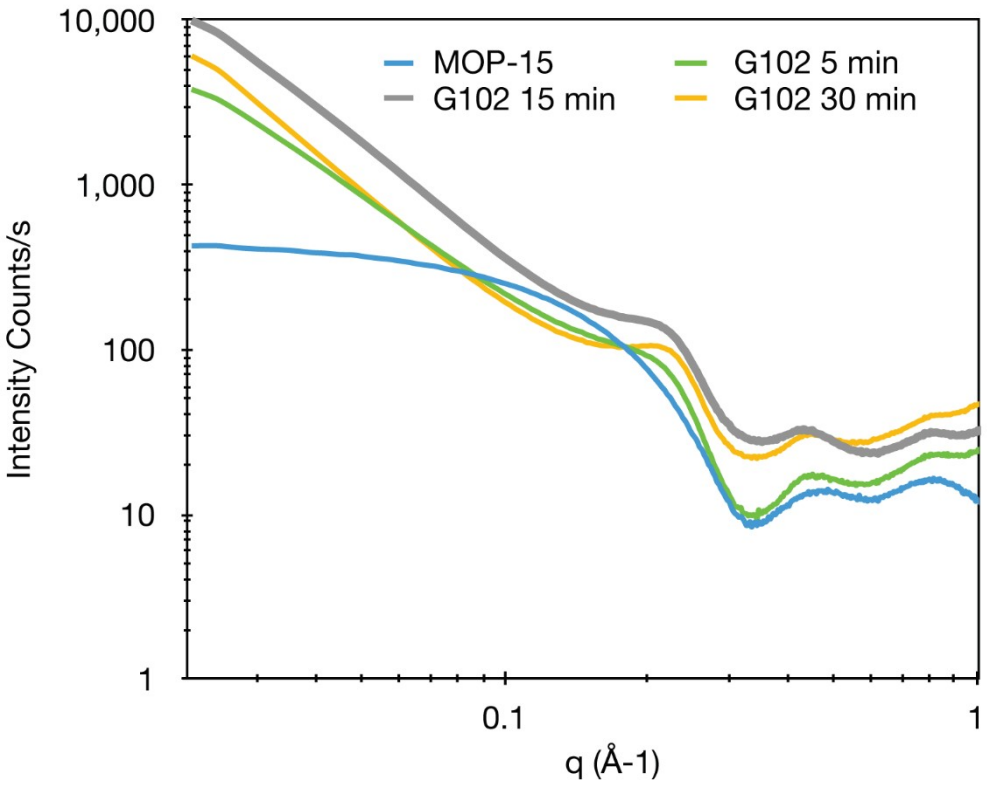

Figure S14. SAXS data monitoring the formation of G102 for 30 minutes in a 3 mm glass capillary.

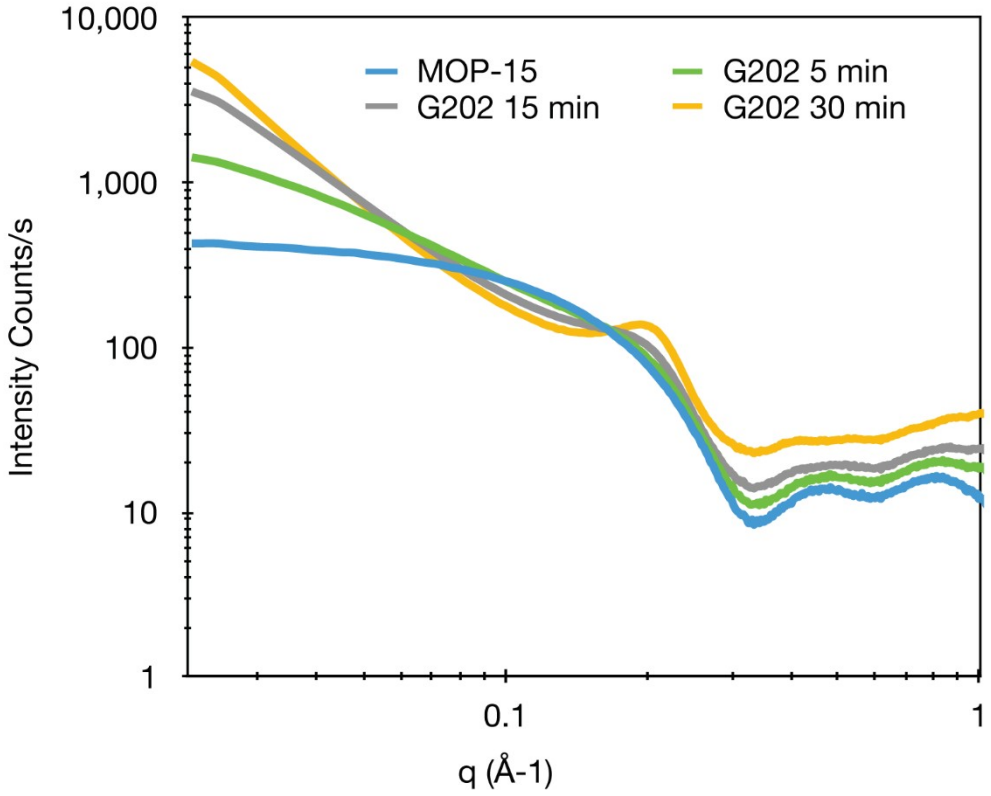

Figure S15. SAXS data monitoring the formation of G202 for 30 minutes in a 3 mm glass capillary.

4. Rheology

All G10X and G20X samples were used as-synthesized for rheological measurements, which were carried out at 25 °C.

4.1. G' and G"; G20X gel series

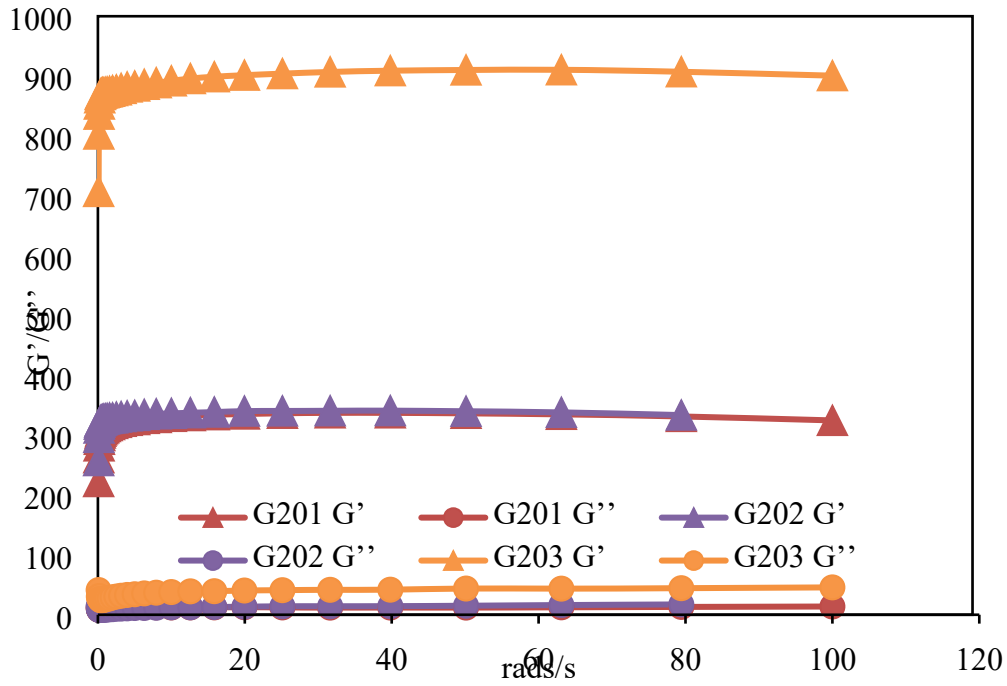

Figure S16. Rheology data G' and G" of the G20X gel samples (G10X data in manuscript).

4.2. Complex viscosity data

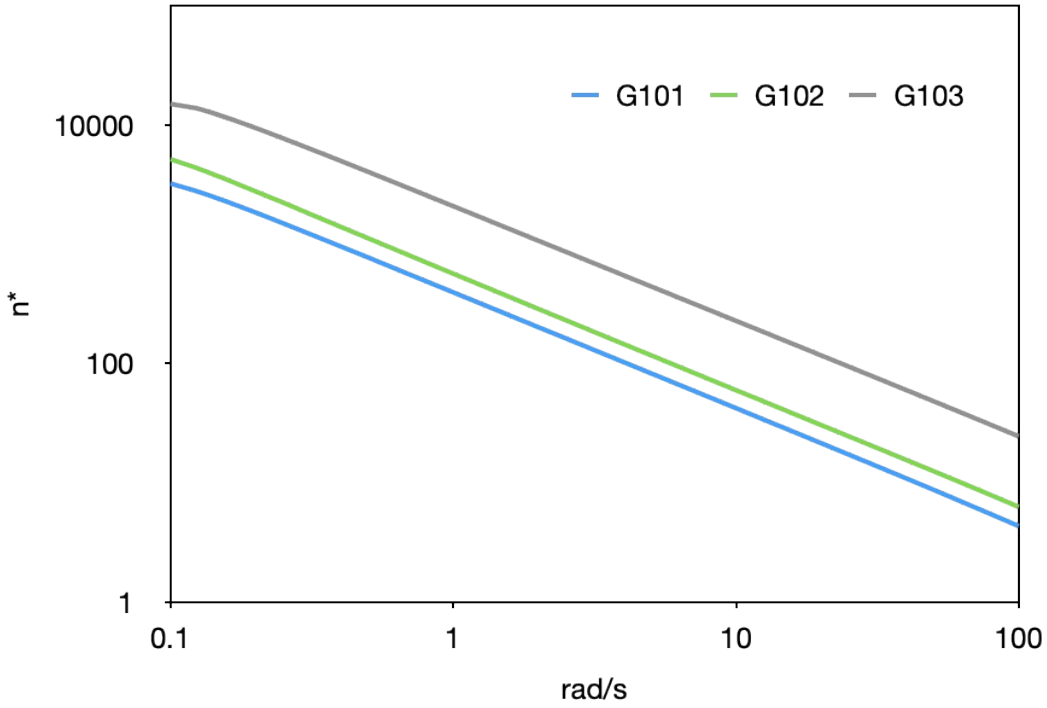

Figure S17. Complex viscosity of the G10X samples.

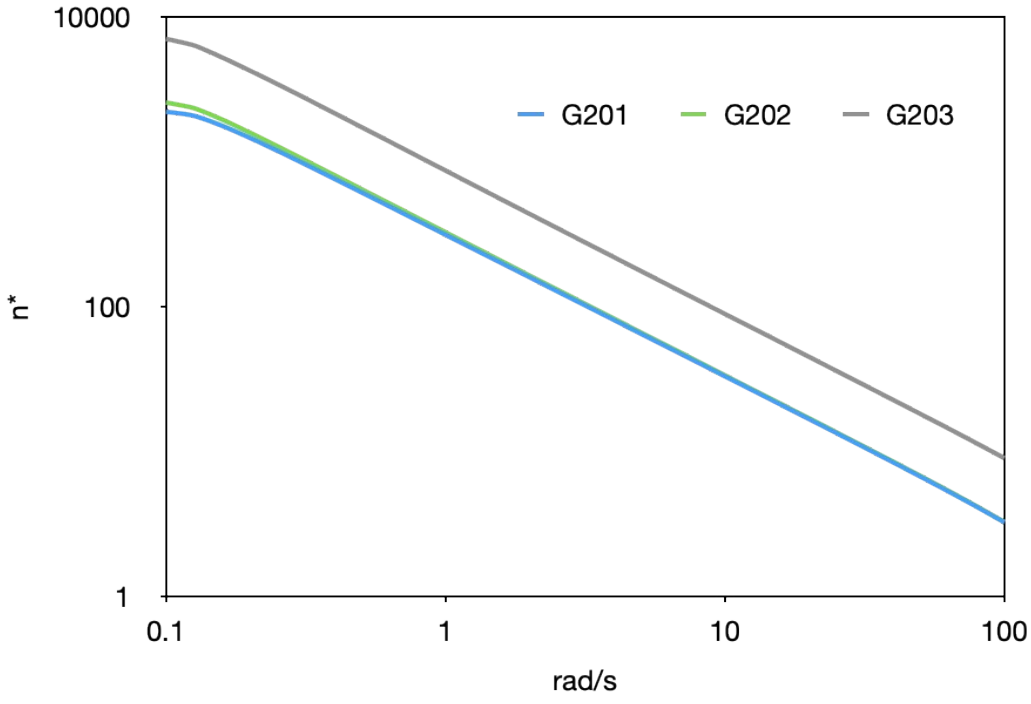

Figure S18. Complex viscosity of the G20X samples.

4.3. Strain sweep data

Strain sweep data was measured in order to select an appropriate strain % for the oscillatory rheological experiments. For example, in Figure S19 strain over 25% results a decline in the G' and G" values. A strain percentage of 5% was therefore utilised for all rheological experiments, which, as shown in Figure S21-S26, falls within an appropriate range.

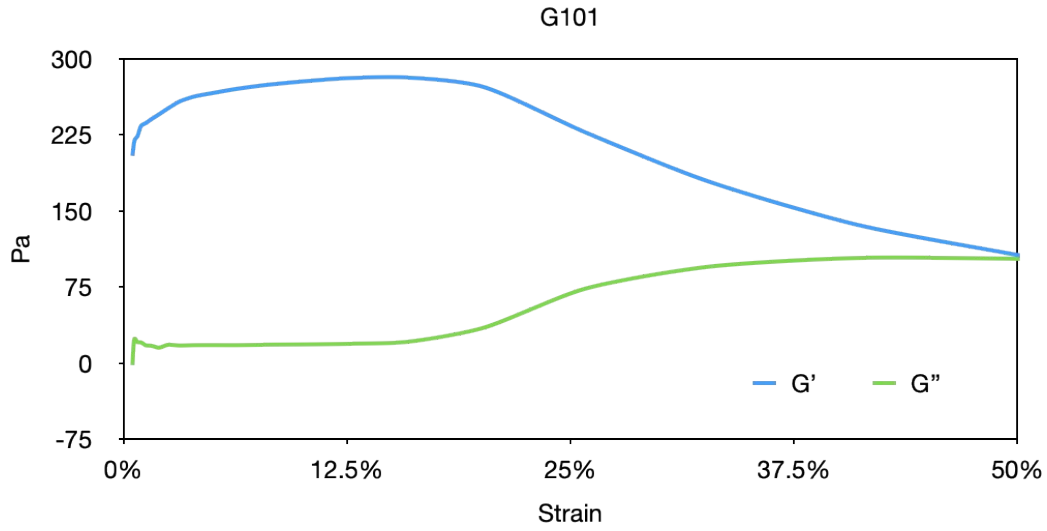

Figure S19. Strain sweep curve for G101.

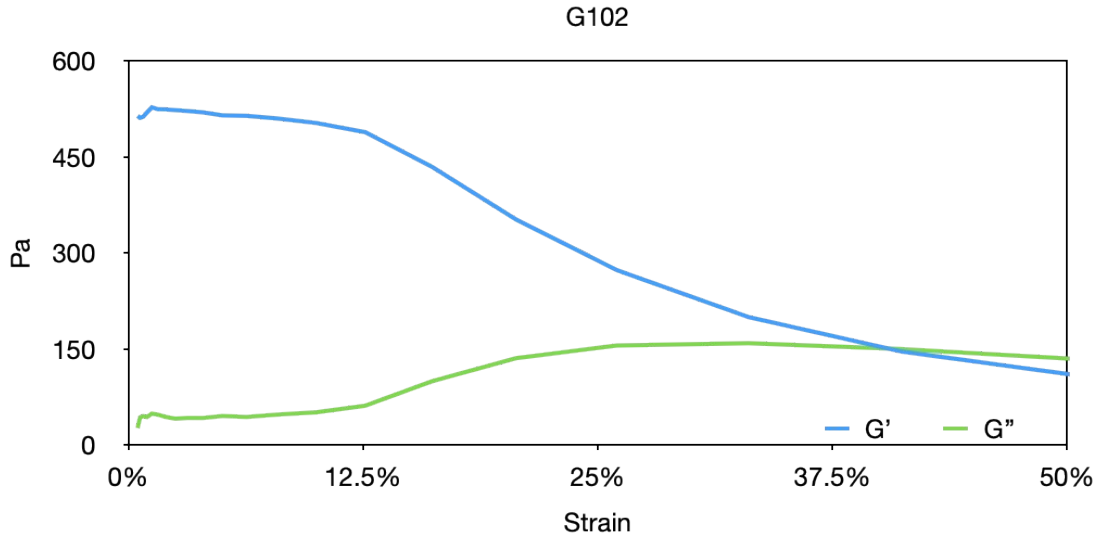

Figure S20. Strain sweep curve for G102.

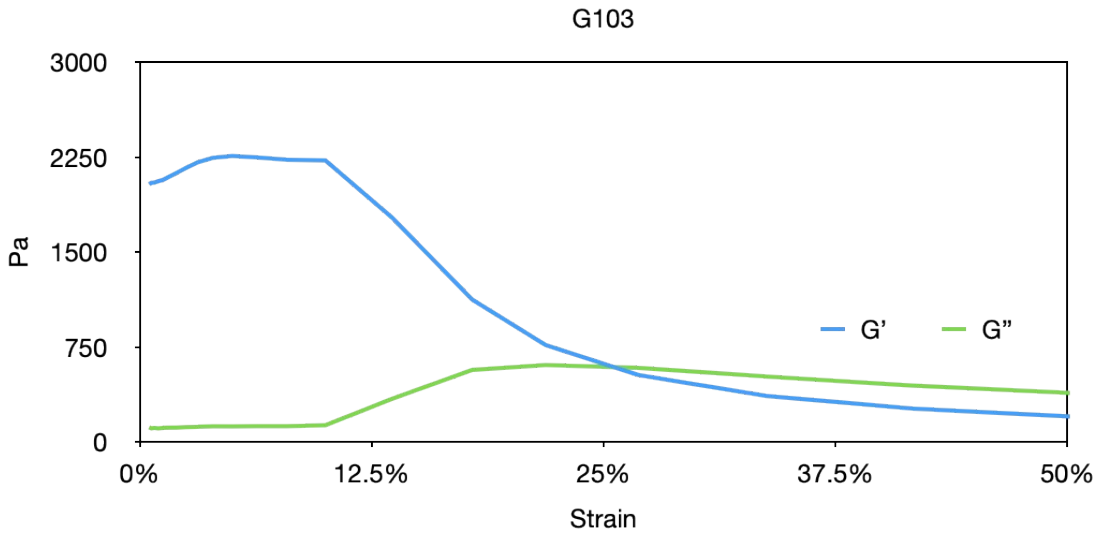

Figure S21. Strain sweep curve for G103.

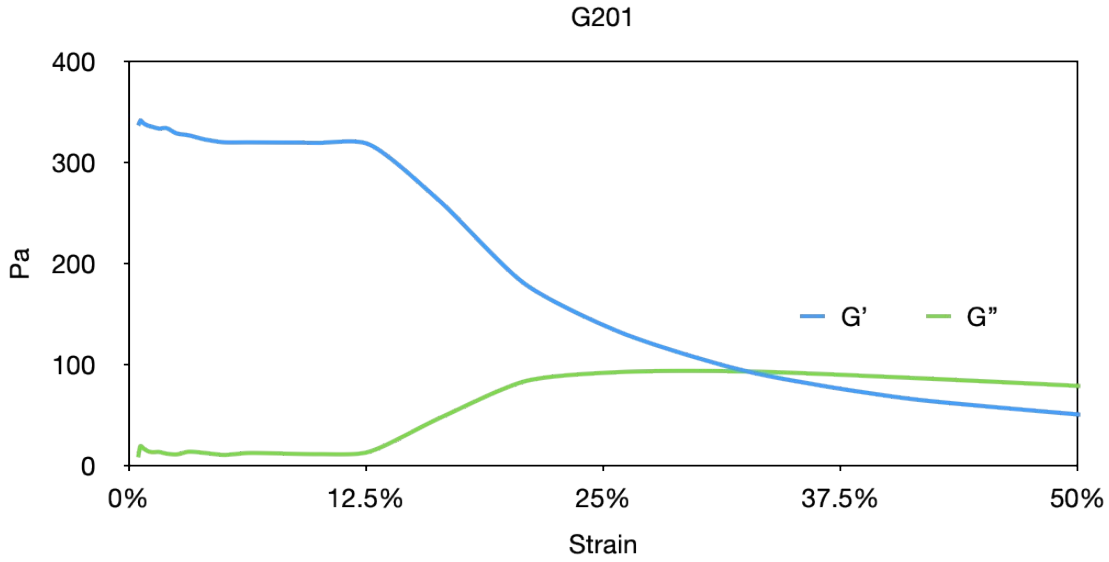

Figure S22. Strain sweep curve for G201.

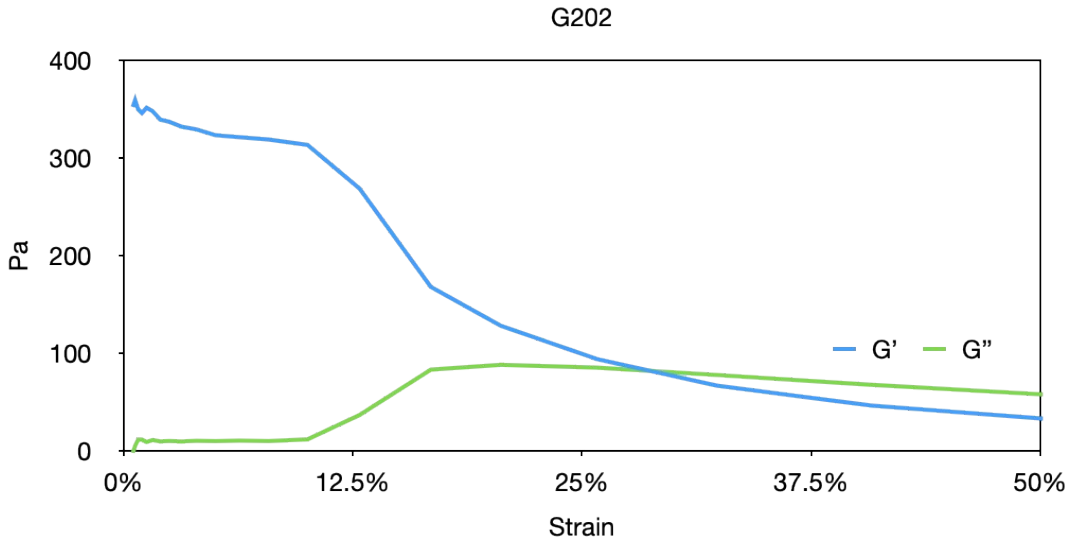

Figure S23. Strain sweep curve for G202.

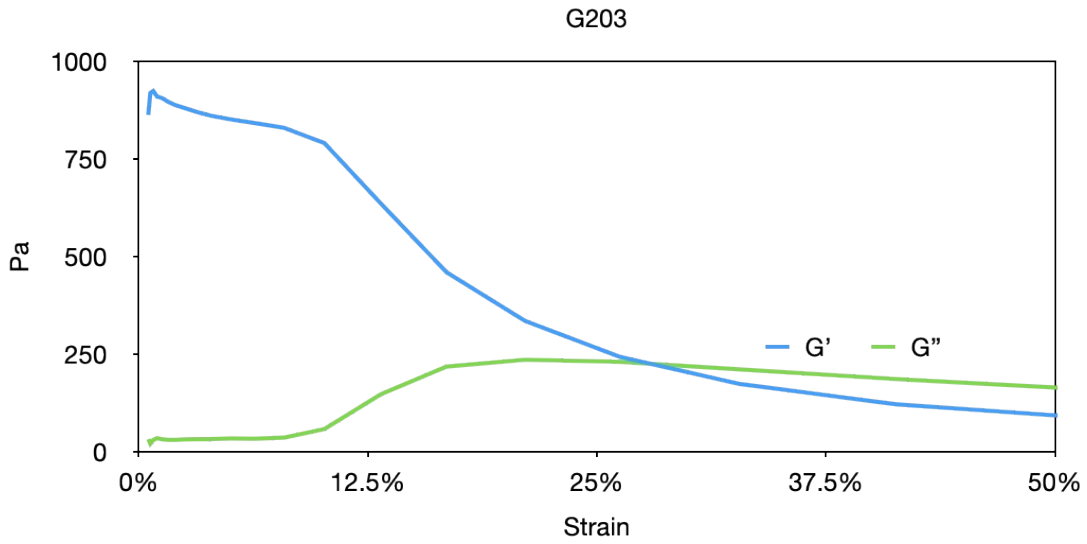

Figure S24. Strain sweep curve for G203.

5. Iodine adsorption data

5.1. I_2 calibration curve

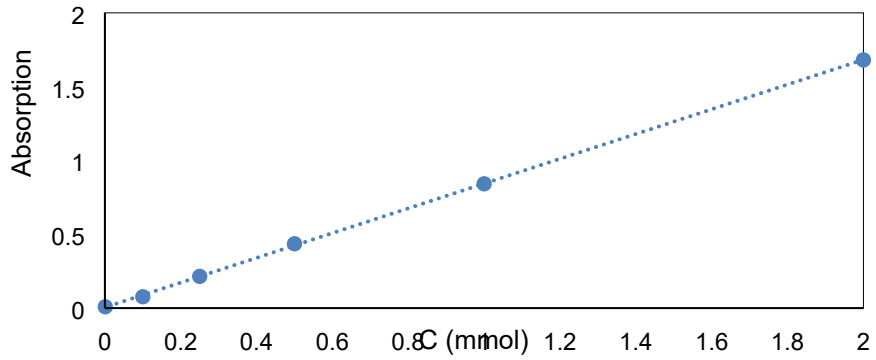

Figure S25. Calibration curve of I_2 concentrations in cyclohexane solution.

5.2. Raw UV-absorption data

The following UV-vis spectra represent the raw data used to calculate the I_2 uptake capacities of G10X and G20X and rates at given time intervals. Quantity of I_2 adsorbed was calculated and expressed as mmol / g, then converted to mg / g.

$$Q(adsorbed) = \frac{C0 - C1}{m} * V$$

Where; C0 = the initial concentration of I_2 in cyclohexane, C1 = Concentration after a given time interval, m = weight of sample (g) and V = volume of I_2 reaction experiment.

All G10X / G20X gels were prepared in dry DMSO on the scale described in section 1.2. Prior to I_2 adsorption, the samples were first subject to solvent exchanged with THF (5 mL x 3). This was done to remove to remove all DMSO and any unreacted aldehyde impurities. The samples were then solvent exchanged with cyclohexane (5 mL x 10) prior to I_2 adsorption. A stock solution of 1.85 mM

I_2 in cyclohexane was utilised for all I_2 adsorption experiments. Figure S26 (below) is an example with a control sample (G106) that shows that the solvent exchange with THF removes free **dfb** and does not alter the branch functionality.

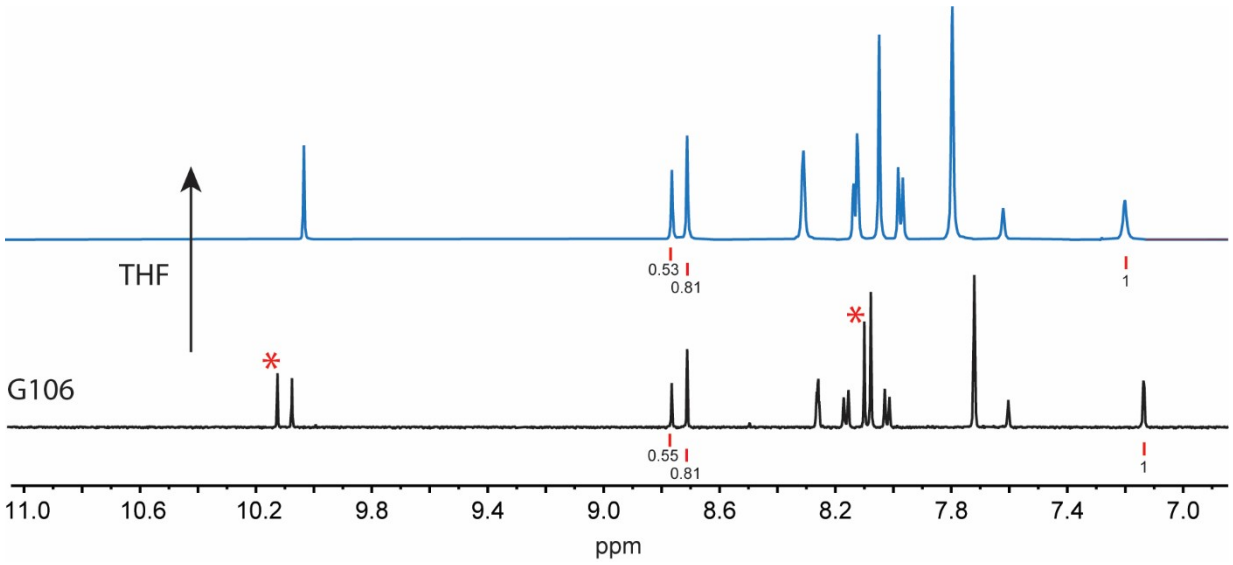

Figure S26. ^{1}H NMR (500 MHz, DMSO-d_6) spectrum of an EGTA digestion of G106 before and after washing with THF. The * indicate that THF washing removes proton resonances of the free dfb whilst not interfering with the imine cross-links. This is evident as the calculated cross-linking of the two samples are 45% and 44% for G106 and G106-THF respectively. This sample (G106) was utilised to exemplify the effect of THF washing on removing dfb and maintaining imine stability.

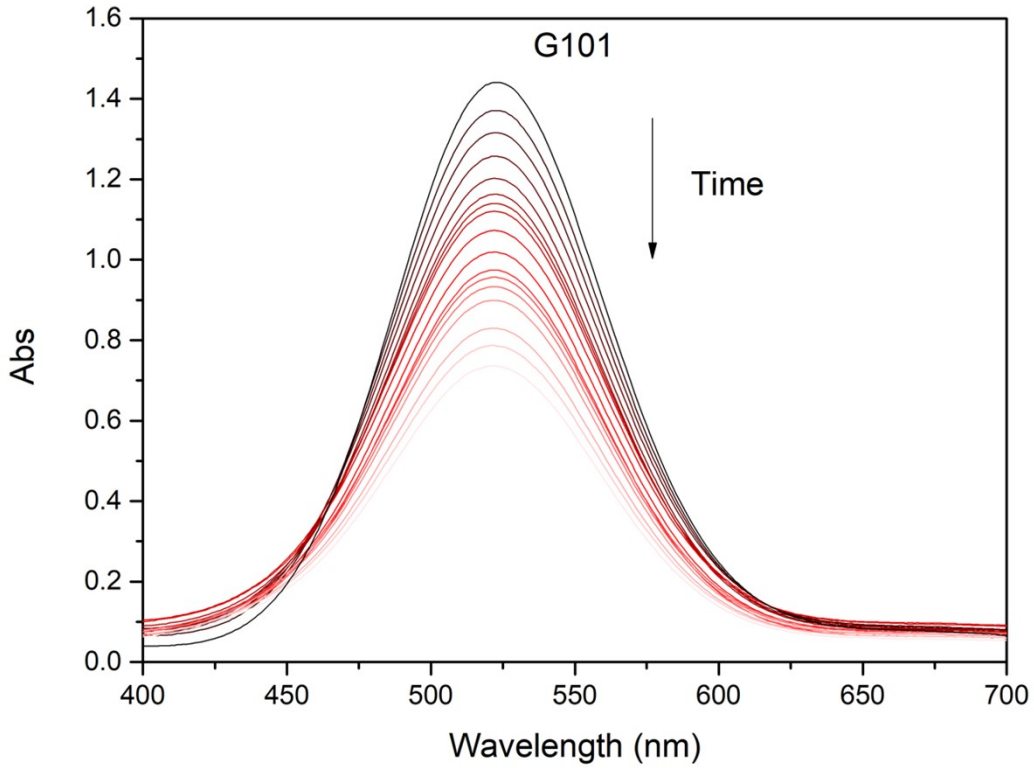

Figure S27. Raw UV-vis data of I_2 absorption in G101.

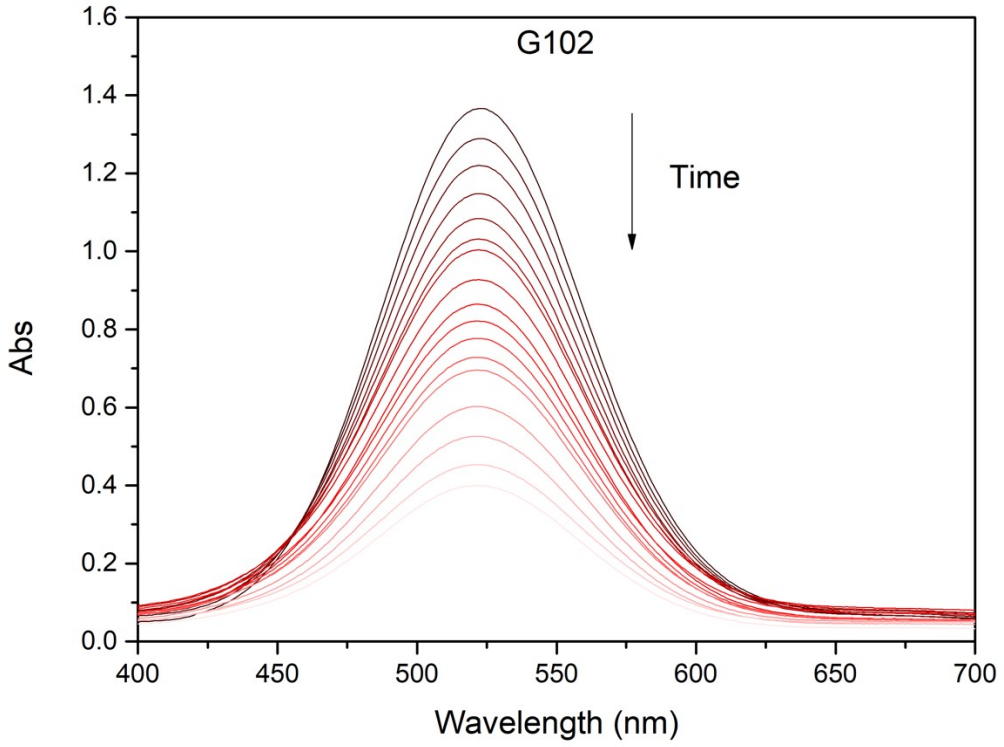

Figure S28. Raw UV-vis data of I_2 absorption in G102.

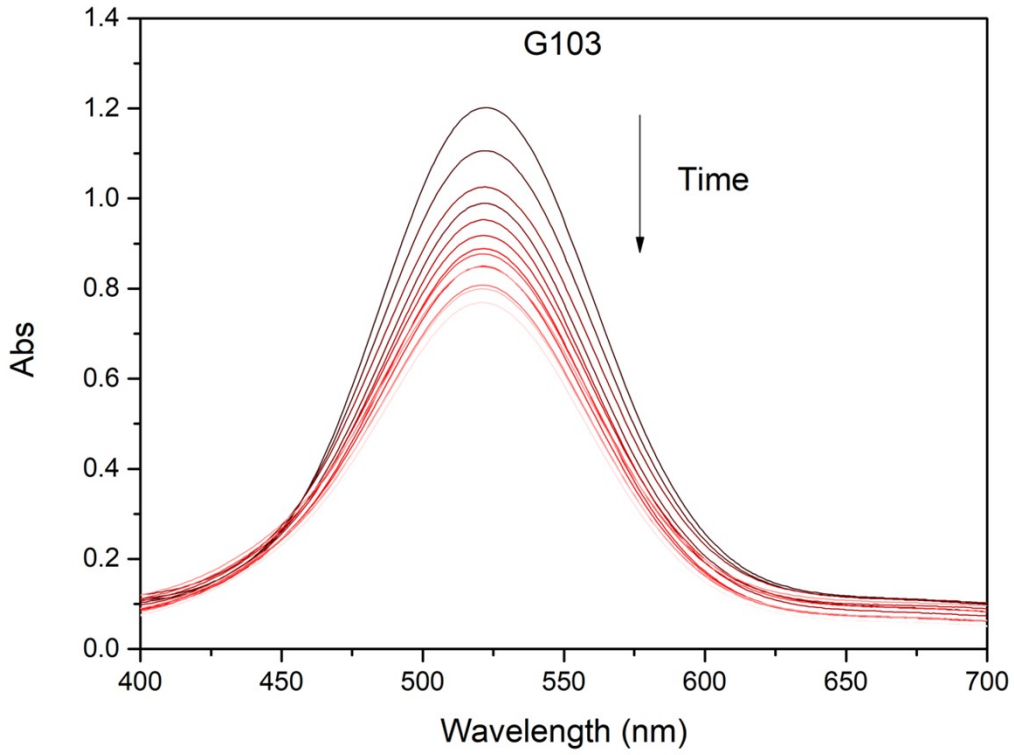

Figure S29. Raw UV-vis data of I_2 absorption in G103.

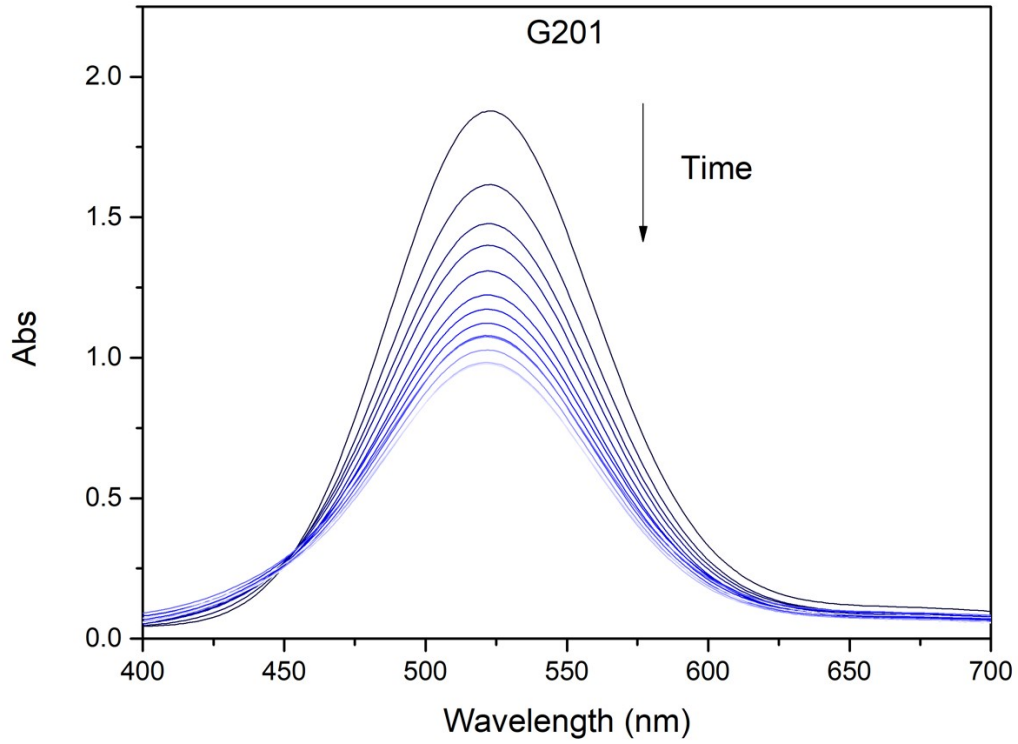

Figure S30. Raw UV-vis data of I_2 absorption in G201.

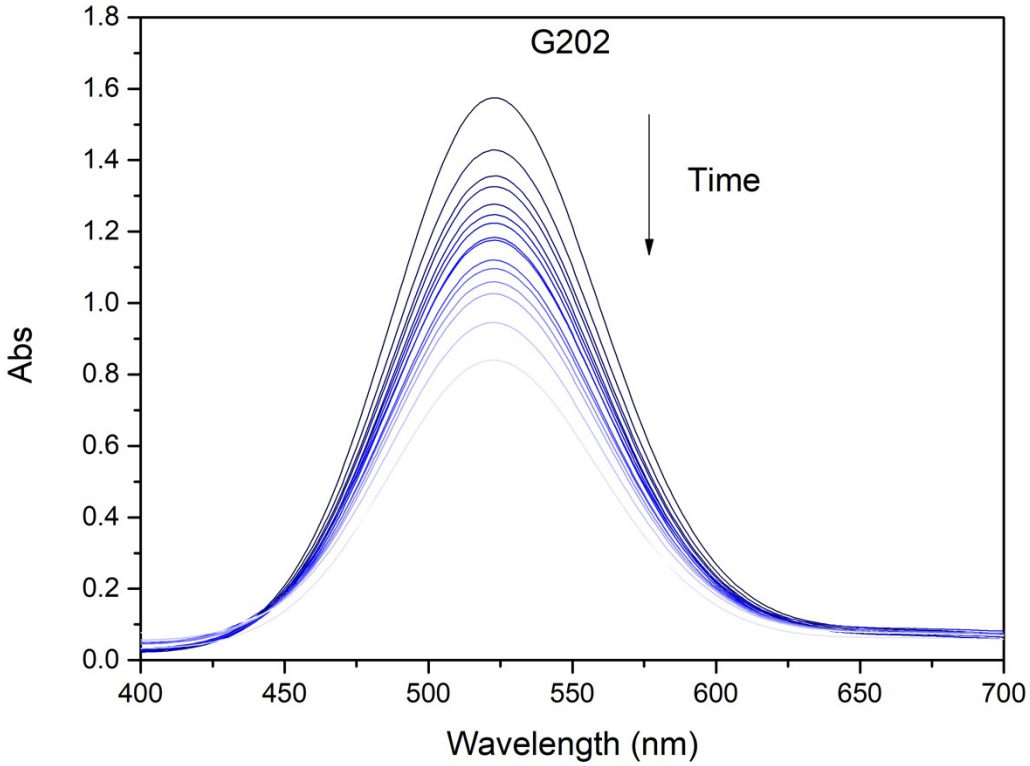

Figure S31. Raw UV-vis data of I_2 absorption in G202.

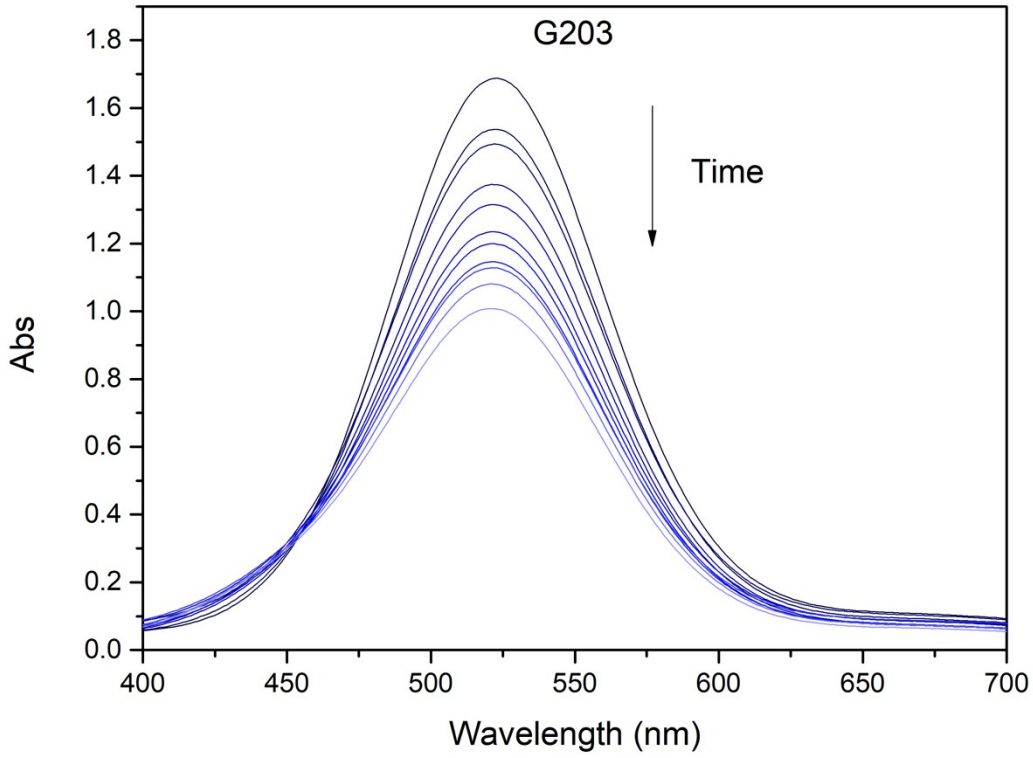

Figure S32. Raw UV-vis data of I_2 absorption in G203.

5.2.1. Rate-data for I_2 uptake

The adsorption rate for the uptake of I_2 into the G10X / G20X system was calculated as first order.[2] The fitting of the data can be viewed below in Figures S35-S36 where the blue data points correspond to the rate from time 0-30 min and the orange data points 30-60 min.

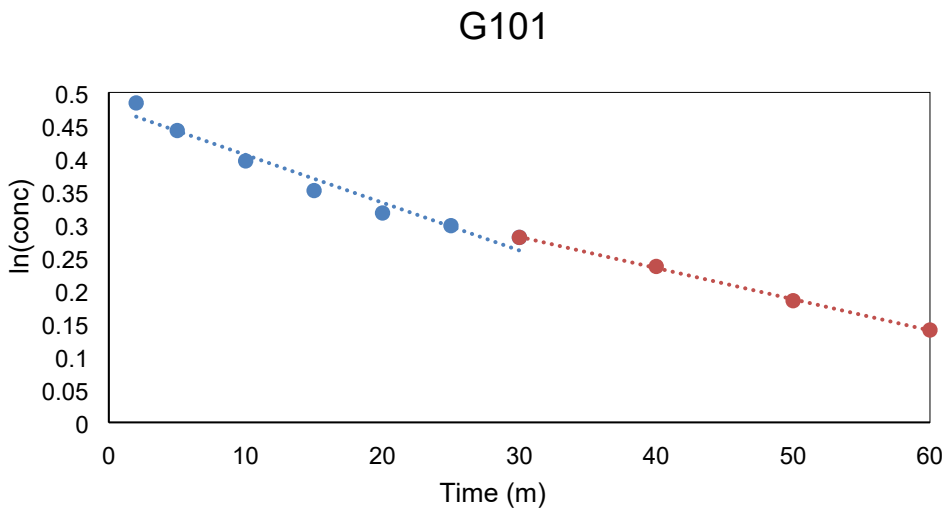

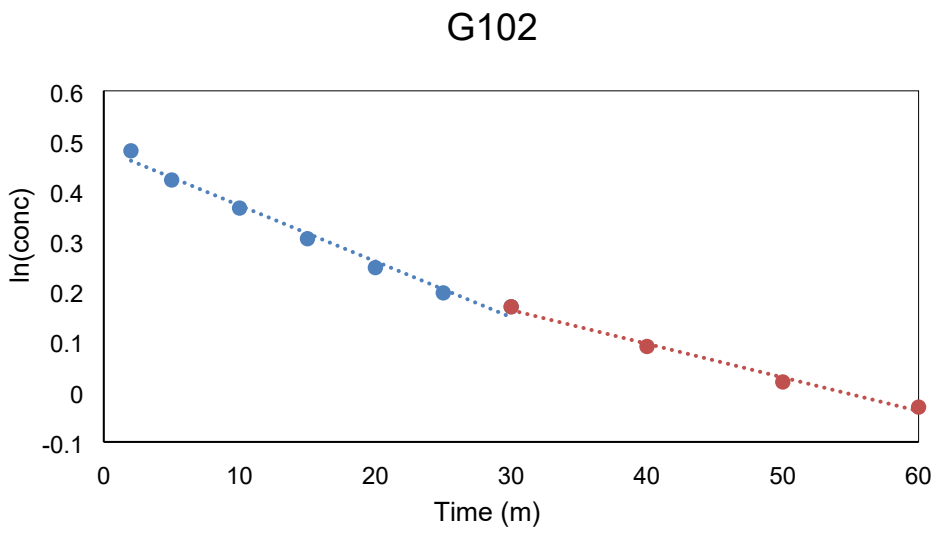

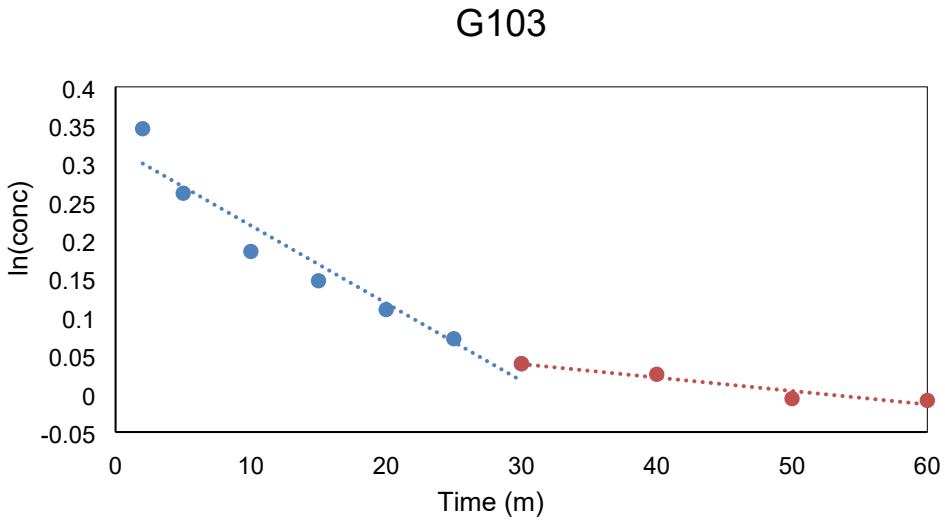

Figure S33. Rate data for the adsorption of I_2 in G101, G102 and G103 from 0-30 minutes (blue) and 30-60 minutes (orange).

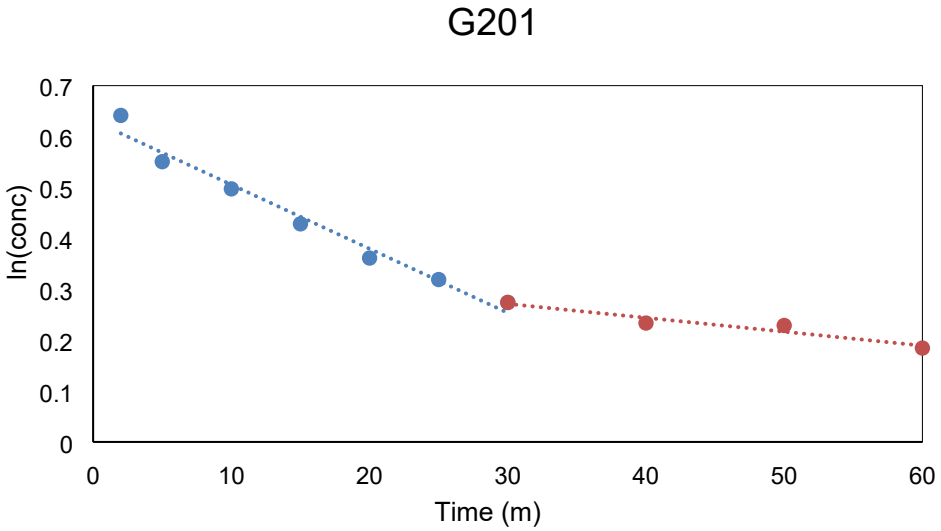

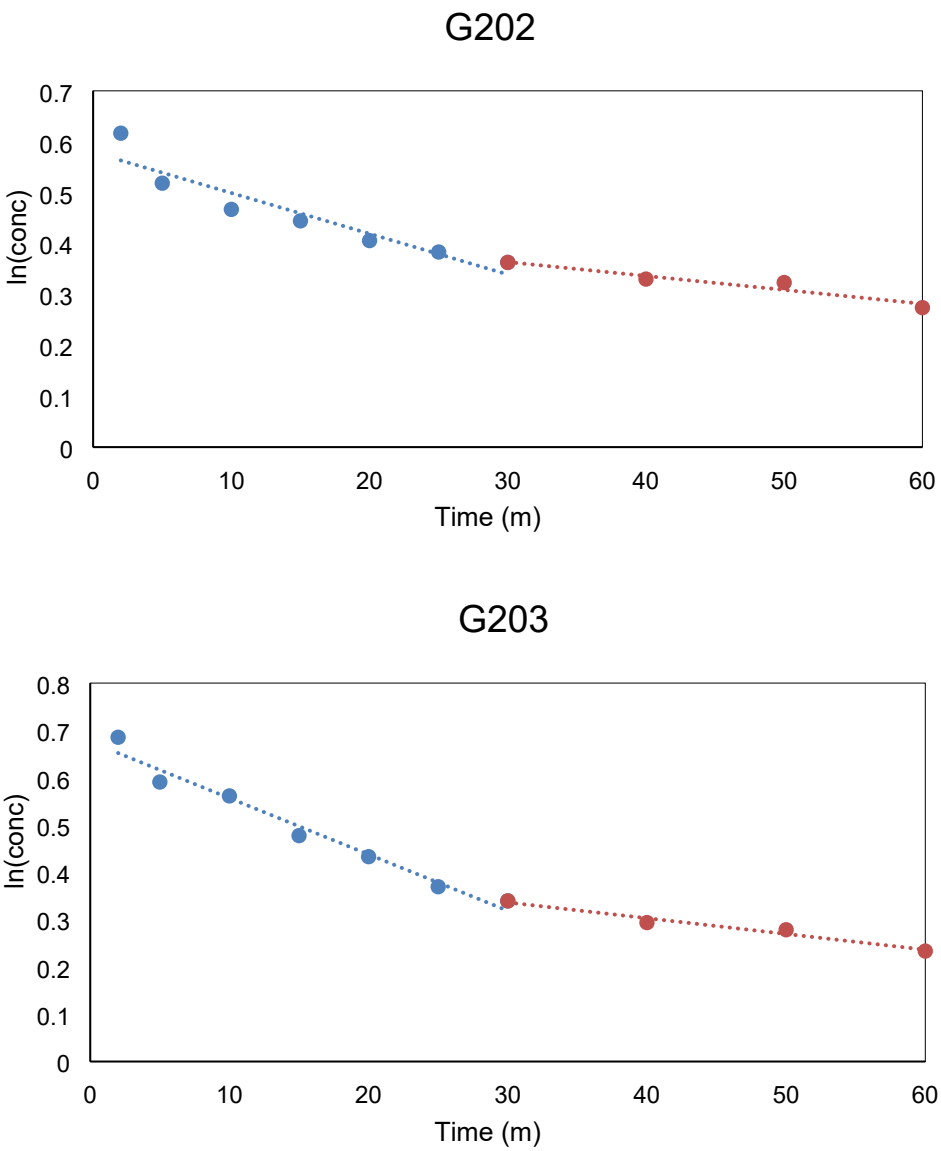

Figure S34. Rate data for the adsorption of I_2 in G201, G202 and G203 from 0-30 minutes (blue) and 30-60 minutes (orange).

Table S4: Calculated adsorption capacity and rate data of the G10X series.

Time	G101		G102		G103	
	Total amount adsorbed (mg/g)	Rate (min^{-1})	Total amount adsorbed (mg/g)	Rate (min^{-1})	Total amount adsorbed (mg/g)	Rate (min^{-1})
30	30	0.0072	44	0.0111	38	0.0101
60	48	0.0047	66	0.0067	43	0.0018

Table S5: Calculated adsorption capacity and rate data of the G20X series.

Time	G201		G202		G203	
	Total amount adsorbed (mg/g)	Rate (min^{-1})	Total amount adsorbed (mg/g)	Rate (min^{-1})	Total amount adsorbed (mg/g)	Rate (min^{-1})
30	59	0.0126	42	0.0080	59	0.0119
60	71	0.0027	55	0.0027	73	0.0033

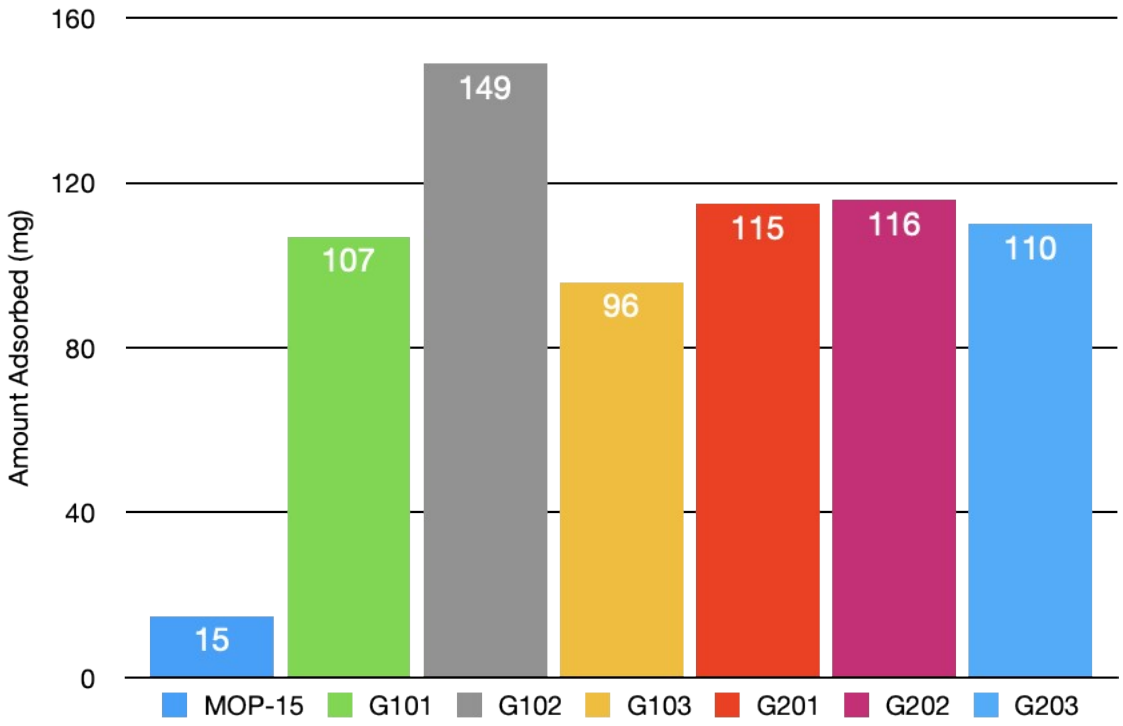

Figure S35. Overall I_2 uptake observed in MOP-15,G10X and G20X samples after 7 days.

5.2.2. *MOP-15 I_2 adsorption data*

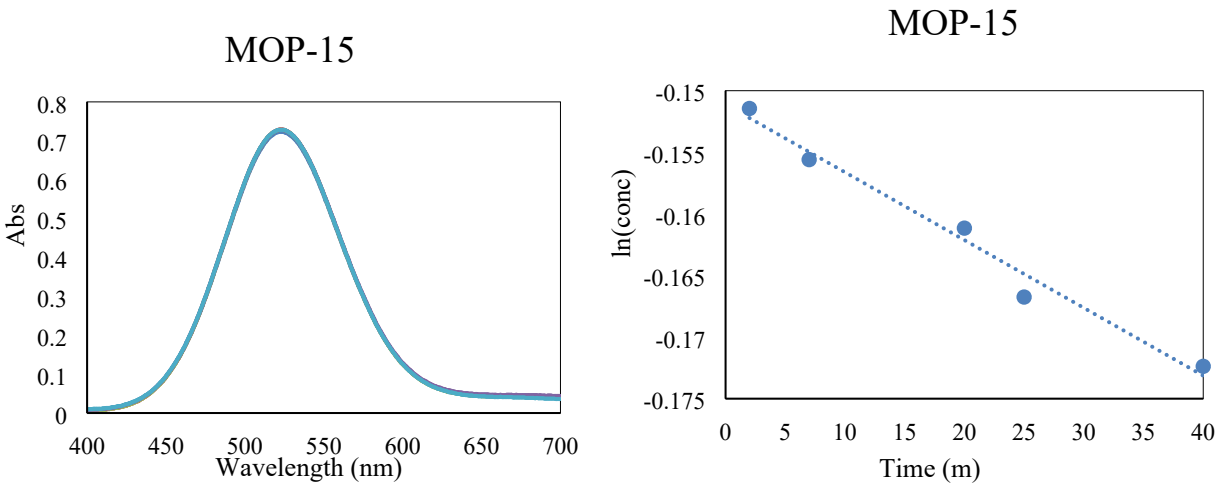

Figure S36. Raw UV-vis data and rate calculation for I_2 adsorption in MOP-15.

5.2.3. *Images of I_2 uptake in MOC polymer networks*

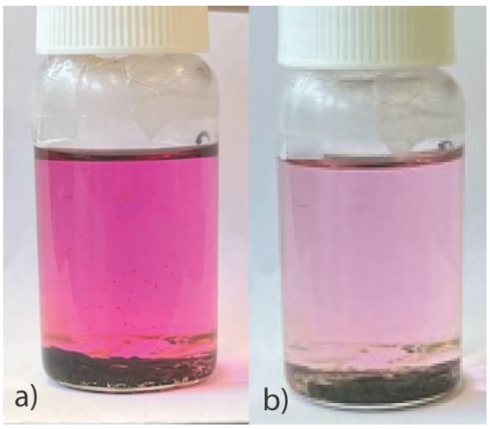

Figure S37. G102 soaked in an I_2 solution of cyclohexane for a) 2 minutes and b) 180 minutes. The reduction in colour intensity corresponds to the adsorption of I_2 from the solution into the sample.

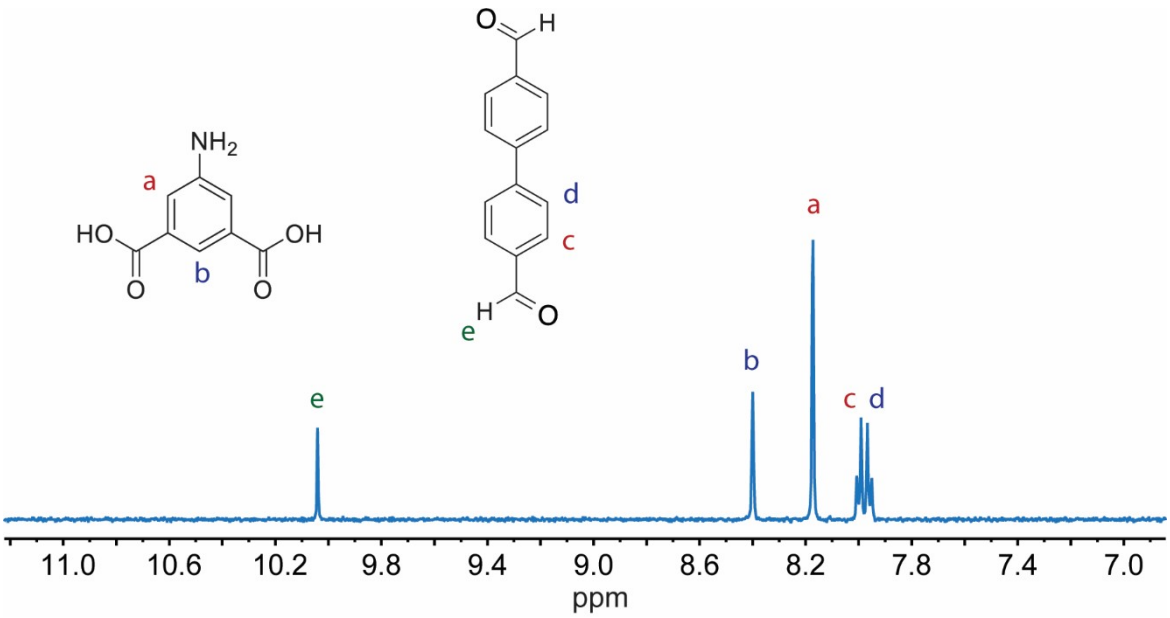

Figure S38. ^{1}H NMR (500 MHz, DMSO-d_6) spectrum of a G20X sample (G202) digested with DCl post I_2 adsorption. The proton signals present relate only to the ligand (5-NH_2-bdc) and **dpc**, indicating that I_2 does not covalently with the gel during adsorption experiments.

Discussion on I_2 interactions within G10X and G20X:

Whilst we cannot exclude the possibility of I_2 adsorbing into the $Cu_{24}L_{24}$ pores of G10X and G20X, there is no direct published evidence to support this. Due to the presence of solvent-filled pores in G10X and G20X and the abundance of amine functional groups, the I_2 uptake and overall capacity is not surprising. Nitrogen rich materials have shown high propensity towards I_2 uptake compared to their unfunctionalized counterparts.[3-7] Moreover, based on previous studies, we expected that I_2 interacts with the π systems of the aromatic rings throughout the gel network.

With regards to interactions with Cu(II) paddlewheels, Chibani and Paul reported Molecular dynamics calculations (DFT / Ab-initio studies) on the I_2 uptake by HKUST-1. They found I_2 to be located in close proximity to the Cu(II) paddlewheel, which may also be the case for G10X and G20X.[8].

6. TEM data of MOP-15 and G10X / G20X

TEM imaging of MOP-15 was performed on an FEI Tecnai G2 Spirit TEM operated at 120 kV. A solution of MOP-15 was added to EtOH before being dispersed onto a carbon TEM grid. TEM imaging of G102 was performed using a probe-corrected, low-base FEI Titan Themis 80-200 (FEI, Hillsboro, OR, USA) operated at 200 kV with an X-FEG Schottky source. A dried sample of G102 was dispersed into EtOH before being loaded onto a carbon TEM grid.

6.1. Transmission Electron Microscopy

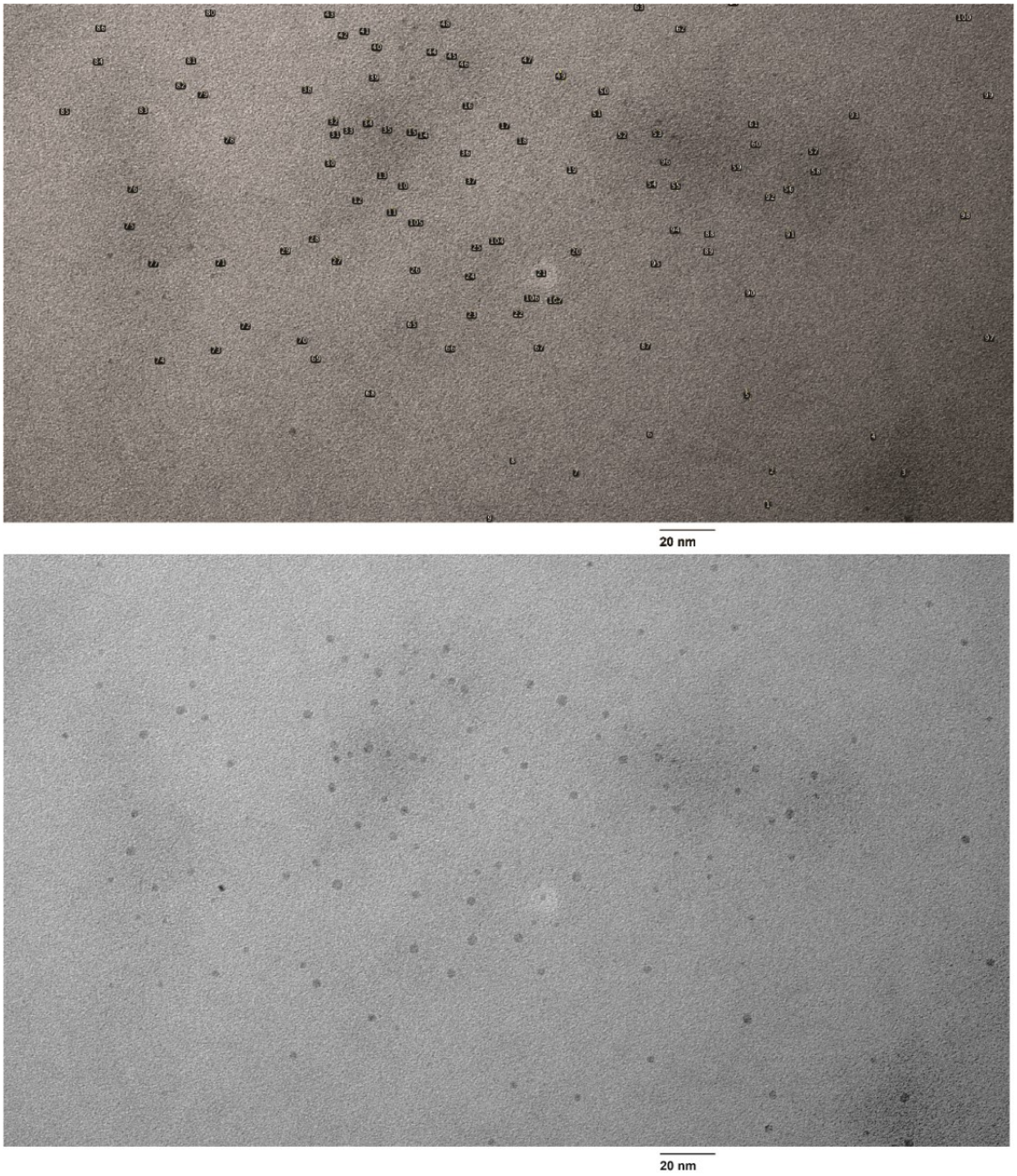

Figure S39. TEM image of MOP-15 labelled (top) and the raw image (bottom), labelled particles were used for calculating particle size distributions.

6.1.1. Size Distribution of MOP-15

The following data was obtained by measuring each individual particle in a set of images taken via TEM. ImageJ was used to measure, calculate, and display the particle distributions.

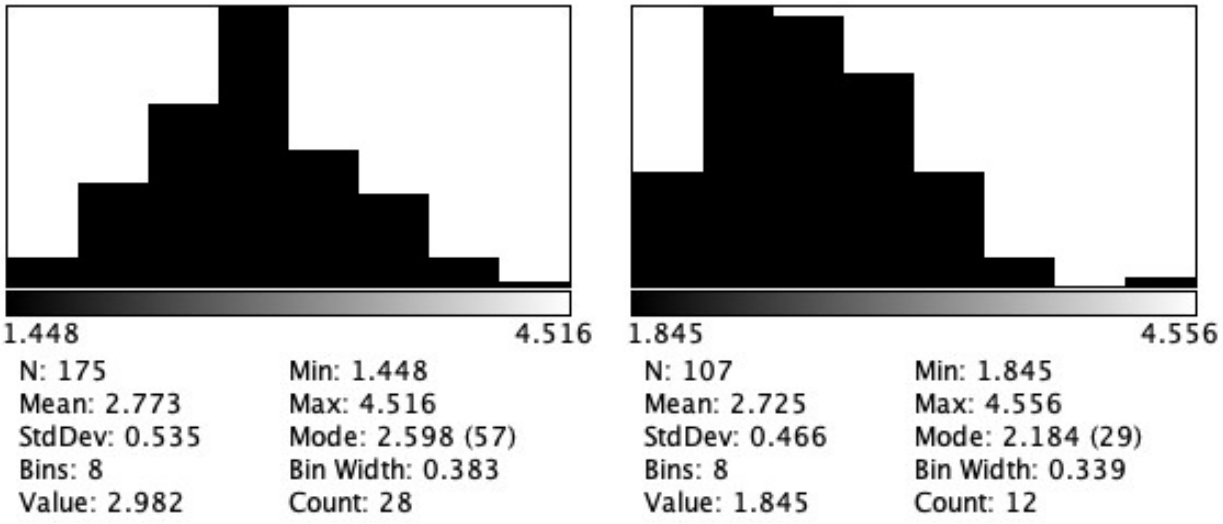

Figure S40. Particle size distributions of MOP-15, the average particle size between both sets of data is similar, being 2.773 nm and 2.725 nm respectively. This size is in good agreement with the expected 2.5 nm size of MOP-15 derived from its crystal structure.

6.1.2. TEM of G102

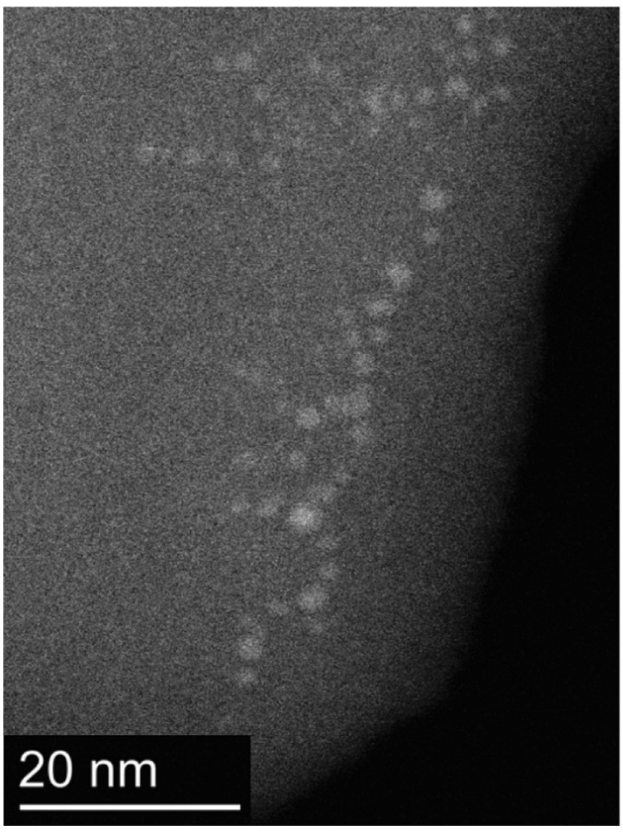

Figure S41. TEM-HAADF image of G102, the particles displayed are further used for calculating particle size distributions.

The following data was obtained by measuring each individual particle in a set of images taken via TEM. ImageJ was used to measure, calculate, and display the particle distributions.

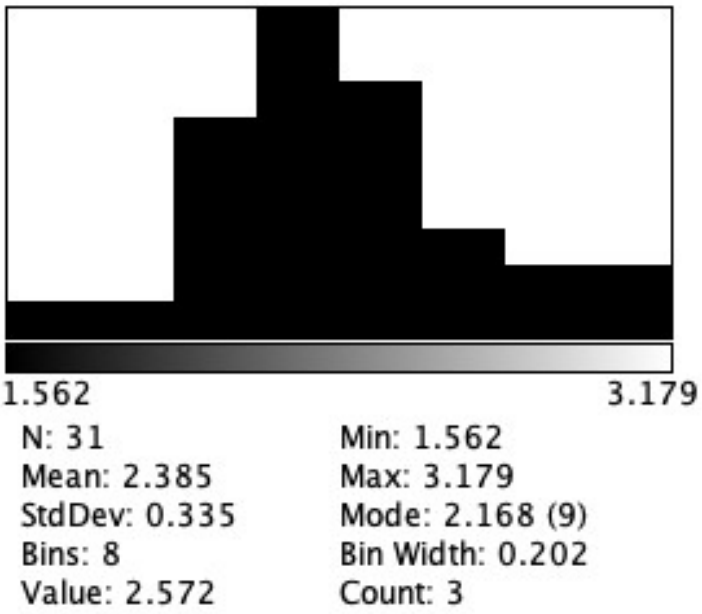

Figure S42. Particle size distributions of cages within G102, the average particle size between both sets is in good agreement with the expected 2.5 nm size of MOP-15 derived from its crystal structure.

7. X-ray crystallography

7.1. General methods

Single crystals were mounted in paratone-N oil on a plastic loop. X-ray diffraction data for **MOP-15·DMSO** and **Cu_{24}(5-MeCONH-bdc)$_{24}$** was collected at 100(2) K on the MX-1 or MX-2 beamline of the Australian Synchrotron.[9,10] Data sets were corrected for absorption using a multi-scan method, and structures were solved by direct methods using SHELXT[11] and refined with SHELXL[12] and ShelXle[13] as a graphical user interface. All non-hydrogen atoms were refined anisotropically and hydrogen atoms were included as invariants at geometrically estimated positions. The contribution of the electron density from disordered, pore-bound solvent molecules, which could not be modelled with discrete atomic positions were handled using the SQUEEZE[14] routine in PLATON,[15] which strongly improved all figures of merit (FOM). X-ray experimental data is given.

Table S6: SQUEEZE results

Structure	**MOP-15·DMSO**	**Cu_{24}(5-MeCONH-bdc)$_{24}$**
_platon_squeeze_void_volume	9372	13918
_platon_squeeze_void_count_electrons	2526	2874
Solvent content	53 DMSO + 30 H_2O molecules	20 DMSO, 113 MeOH

*7.1.1. Specific refinement details for **MOP-15·DMSO***

The refinement of ADP's for carbon, nitrogen and oxygen atoms was aided by similarity restraints (SIMU).[16] Stereochemical restraints for DMSO solvent molecules were generated by the GRADE program using the GRADE Web Server (http://grade.globalphasing.org) and applied in the refinement. A GRADE dictionary for SHELXL contains target values and standard deviations for 1,2-

distances (DFIX) and 1,3-distances (DANG), as well as restraints for planar groups (FLAT). This help to produce a stable model of the coordinated DMSO solvent.

7.1.2. Specific refinement details for Cu_{24}*(5-MeCONH-bdc)*$_{24}$

The refinement of ADP's for carbon, nitrogen and oxygen atoms was aided by similarity restraints (SIMU).[16] Stereochemical restraints for amide ligand molecules were generated by the GRADE program using the GRADE Web Server (http://grade.globalphasing.org) and applied in the refinement. A GRADE dictionary for SHELXL contains target values and standard deviations for 1,2-distances (DFIX) and 1,3-distances (DANG), as well as restraints for planar groups (FLAT). This help to produce a stable model of the disordered amide moiety of the ligand.

Table S7: X-ray experimental data

Compound	**MOP-15·DMSO**	**Cu_{24}(5-MeCONH-bdc)$_{24}$**
CCDC number	2193899	2193900
Empirical formula	$C_{216}H_{216}Cu_{24}N_{24}O_{120}S_{12}$	$C_{248}H_{186}Cu_{24}N_{24}O_{146}$
Formula weight	6953.60	7363.16
Crystal system	Triclinic	Orthorhombic
Space group	P-1	*Pnnm*
a (Å)	25.196(5)	32.745(7)
b (Å)	25.765(5)	25.599(5)
c (Å)	26.927(5)	30.565(6)
α (º)	108.23	90°
β (º)	103.21	90°
γ (º)	111.69	90°
Volume (Å^3)	14204(6)	25621(9)
Z	1	2
Density (calc.) (Mg/m^3)	0.813	0.954
Absorption coefficient (mm^{-1})	0.969	1.034
F(000)	3504	7408
Crystal size (mm^3)	0.40 x 0.13 x 0.11	0.18 x 0.13 x 0.12
θ range for data collection (º)	0.865 to 24.407	0.911 to 24.112
Reflections collected	157366	269331
Observed reflections [R(int)]	43770 [0.0391]	20776 [0.0320]
Goodness-of-fit on F^2	1.250	1.608
R_1 [I>2σ(I)]	0.0914	0.1098
wR_2 (all data)	0.3377	0.3728
Largest diff. peak and hole (e.Å-3)	1.360 and -0.668	1.360 and -0.941
Data / restraints / parameters	43770 / 3338 / 1895	20776 / 1189 / 1104

7.2. Thermal ellipsoid plots

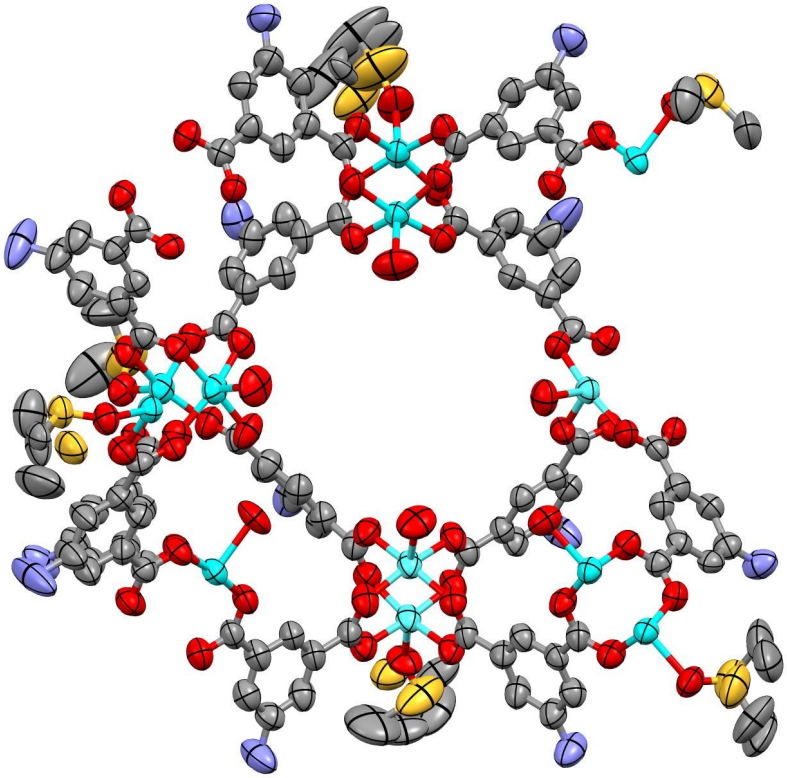

Figure S43. The asymmetric unit of **MOP-15·DMSO** with all non-hydrogen atoms shown as ellipsoids at the 50% probability level.

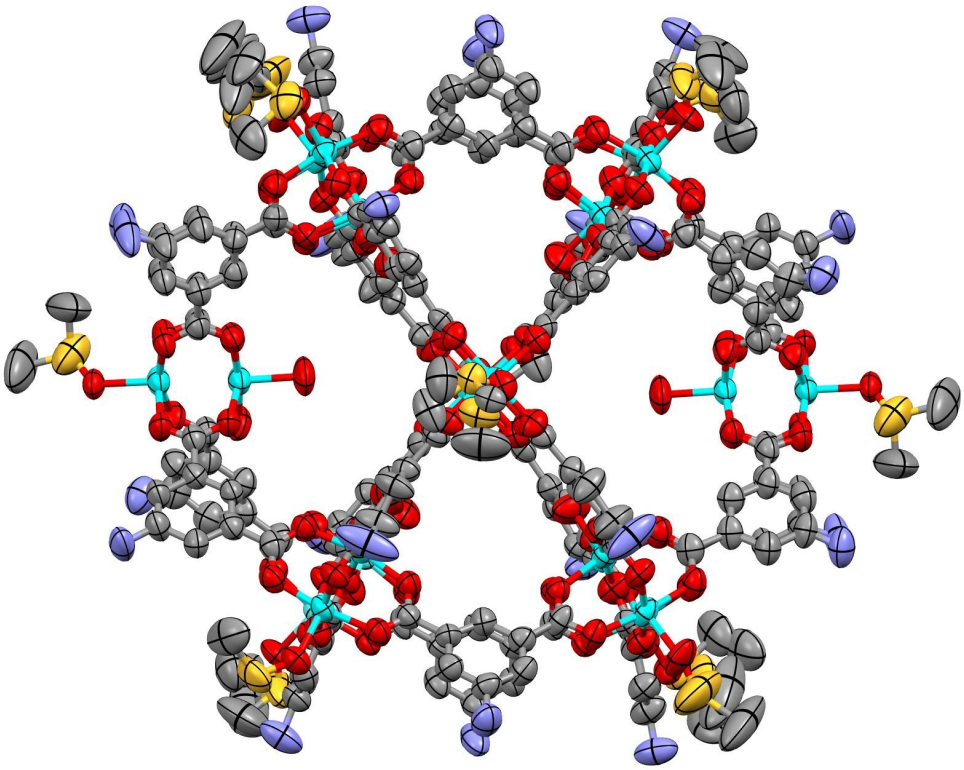

Figure S44. MOP-15·DMSO with all non-hydrogen atoms shown as ellipsoids at the 50% probability level.

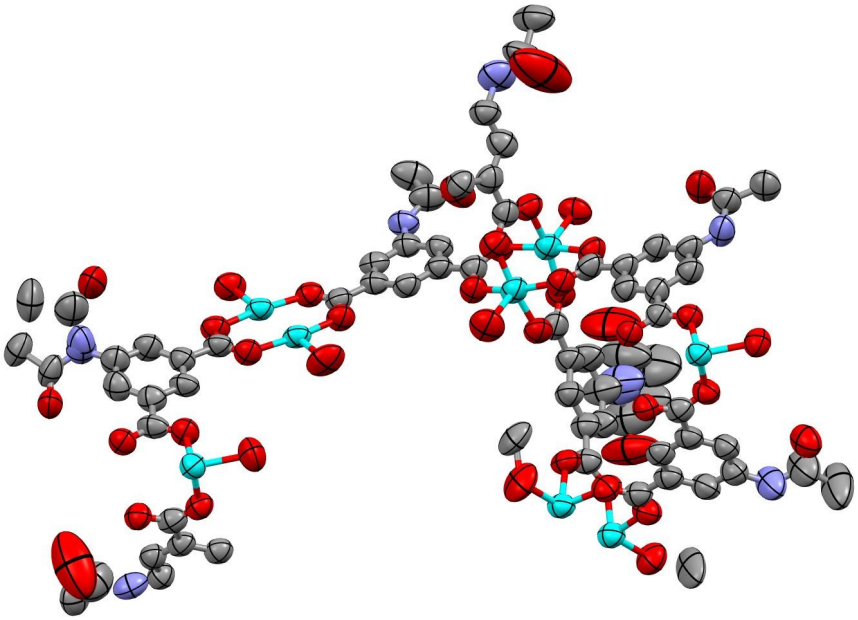

Figure S45. The asymmetric unit of **Cu_{24}(5-MeCONH-bdc)$_{24}$** with all non-hydrogen atoms shown as ellipsoids at the 50% probability level.

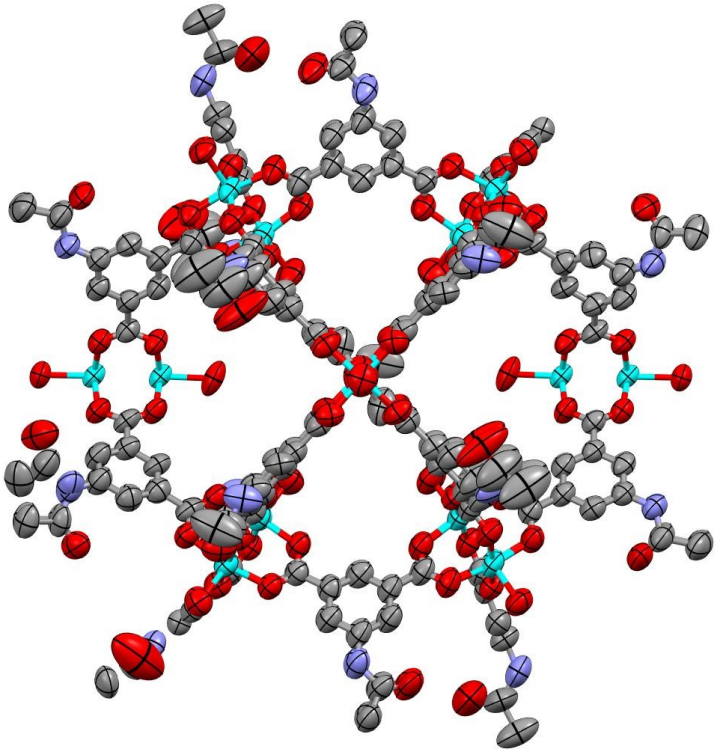

Figure S46. Cu_{24}(5-MeCONH-bdc)$_{24}$ with all non-hydrogen atoms shown as ellipsoids at the 50% probability level.

8. References

1 H. Furukawa, J. Kim, N. W. Ockwig, M. O'Keeffe and O. M. Yaghi, *J. Am. Chem. Soc.*, 2008, **130**, 11650–11661.

2 E. Amayuelas, A. Fidalgo-Marijuán, B. Bazán, M.-K. Urtiaga, G. Barandika and M.-I. Arriortua, *CrystEngComm*, 2016, **18**, 1709–1712.

3 W. Xie, D. Cui, S.-R. Zhang, Y.-H. Xu and D.-L. Jiang, *Mater. Horizons*, 2019, **6**, 1571–1595.

4 C. Falaise, C. Volkringer, J. Facqueur, T. Bousquet, L. Gasnot and T. Loiseau, *Chem. Commun.*, 2013, **49**, 10320–10322.

5 P. Chen, X. He, M. Pang, X. Dong, S. Zhao and W. Zhang, *ACS Appl. Mater. Interfaces*, 2020, **12**, 20429–20439.

6 X. Zhang, J. Maddock, T. M. Nenoff, M. A. Denecke, S. Yang and M. Schröder, *Chem. Soc. Rev.*, 2022, **51**, 3243–3262.

7 G. Q. Wang, J. F. Huang, X. F. Huang, S. Q. Deng, S. R. Zheng, S. L. Cai, J. Fan and W. G. Zhang, *Inorg. Chem. Front.*, 2021, **8**, 1083–1092.

8 S. Chibani, F. Chiter, L. Cantrel and J. F. Paul, *J. Phys. Chem. C*, 2017, **121**, 25283–25291.

9 N. P. Cowieson, D. Aragao, M. Clift, D. J. Ericsson, C. Gee, S. J. Harrop, N. Mudie, S. Panjikar, J. R. Price, A. Riboldi-Tunnicliffe, R. Williamson and T. Caradoc-Davies, *J. Synchrotron Radiat.*, 2015, **22**, 187–190.

10 D. Aragao, J. Aishima, H. Cherukuvada, R. Clarken, M. Clift, N. P. Cowieson, D. J. Ericsson, C. L. Gee, S. Macedo, N. Mudie, S. Panjikar, J. R. Price, A. Riboldi-Tunnicliffe, R. Rostan, R. Williamson and T. T. Caradoc-Davies, *J. Synchrotron Radiat.*, 2018, **25**, 885–891.

11 G. M. Sheldrick, *Acta Crystallogr. Sect. A*, 2015, **71**, 3–8.

12 G. M. Sheldrick, *Acta Crystallogr. Sect. C*, 2015, **71**, 3–8.

13 C. B. Hubschle, G. M. Sheldrick and B. Dittrich, *J. Appl. Crystallogr.*, 2011, **44**, 1281–1284.

14 A. Spek, *Acta Crystallogr. Sect. C*, 2015, **71**, 9–18.

15 A. Spek, *Acta Crystallogr. Sect. D*, 2009, **65**, 148–155.

16 A. Thorn, B. Dittrich and G. M. Sheldrick, *Acta Crystallogr. Sect. A*, 2012, **68**, 448–451.